Czech Technical University in Prague
Faculty of Electrical Engineering
Department of Circuit Theory

Master's thesis

Ondrej Krivosudský

Praha – 2014

Czech Technical University in Prague
Faculty of Electrical Engineering
Department of Circuit Theory

Microwave absorption and permittivity of protein and microtubule solution

Master's thesis

Author: **Ondrej Krivosudský**
Supervisor: **Ing. Ladislav Oppl, Ph.D.**
Supervisor specialist: **Ing. Michal Cifra, Ph.D.**
School Year: **2013/2014**

České vysoké učení technické v Praze
Fakulta elektrotechnická

Katedra teorie obvodů

ZADÁNÍ DIPLOMOVÉ PRÁCE

Student: Bc. Ondrej K r i v o s u d s k ý

Studijní program: Biomedicínské inženýrství a informatika (magisterský)

Obor: Biomedicínské inženýrství

Název tématu: Mikrovlnná absorpce a permitivita roztoku proteinů a mikrotubulů

Pokyny pro vypracování:

1. Připravte přehled problematiky frekvenční závislosti permitivity roztoku vody a proteinů a elektromagnetických vlastností biologických proteinových polymerů – mikrotubulů.
2. Vytvořte model dielektrické disperze roztoku vody a proteinů.
3. Vytvořte model absorpce elektromagnetického pole mikrotubuly s využitím inženýrského anténářského i fyzikálního molekulárního přístupu.
4. Vyhotovte parametrickou analýzu mikrovlnné absorpce mikrotubulů.
5. Experimentálně ověřte permitivitu roztoku vody a proteinů.

Odborný konzultant: Ing. Michal Cifra, Ph.D.

Seznam odborné literatury:

[1] Novotný, K. :Teorie elektromagnetického pole II. ČVUT, Praha, 1997.
[2] Sedlák, B.; Štoll, I.: Elektřina a magnetismus. Karolinum, 2012.
[3] Pechač, P.; Mazánek, M.: Šíření elektromagnetických vln a antény. ČVUT, 2008.
[4] Stracke, R.; Bohm, K. J.; Wollweber, L.; Tuszynski, J. A.; Unger, E.: Analysis of the migration behaviour of single microtubules in electric fields. Biochemical and Biophysical Research Communications, 293(1):602-8211;609, 2002.
[5] Brown, J. A. M.: A Study of the Interactions between Electromagnetic Fields and Microtubules: Ferroelectric Efects, Signal Transduction and Electronic Conduction. Doctoral thesis, University of Alberta, Edmonton Alberta, 1999.

Vedoucí diplomové práce: Ing. Ladislav Oppl, Ph.D.

Platnost zadání: do konce letního semestru 2014/2015

L.S.

prof. Ing. Pavel Sovka, CSc.
vedoucí katedry

prof. Ing. Pavel Ripka, CSc.
děkan

V Praze dne 10. 1. 2014

Prehlásenie

Prehlasujem, že som predloženú prácu vypracoval samostatne a že som uviedol všetky použité informačné zdroje v súlade s Metodickým pokynom o dodržovaní etických princípov pri príprave vysokoškolských záverečných prác.

V Prahe dňa ..... Podpis autora práce .....

Prehlásenie o súhlase

Prehlasujem, že súhlasím s použitím tohoto školského diela fakultou v zmysle § 60 Zákona č. 121/2000 Sb., o právu autorskom, o právach súvisejúcich s právom autorským a o zmene niektorých zákonov - autorský zákon.

Declaration

I hereby state that the given thesis has been written and formulated by me and by me only and that I have cited all used sources in accordance with Metodical assignments of upholding ethical principles during the formulation of university final theses.

Abstract

Purpose: Theoretical study and calculation of microwave absorption in biological protein structure together with theoretical and experimental investigation of protein influence on a complex permittivity in aqueous solution.

Materials and Methods: Microwave absorption by microtubules has been calculated. Key parameters of microtubules absorption were determined by using molecular and physical approaches. The basic concept of protein behavior along with its effect on complex permittivity in aqueous environment was investigated. Agilent Dielectric Probe Kit with slim probe was used for measuring complex permittivity of proteins in solutions. The purpose is to describe dielectric and electromagnetic properties of proteins, so we can gain deeper understanding of their interaction with electromagnetic field and their possible role in generation of electromagnetic field.

Results and Conclusion: Calculations have shown that microtubule absorption is mainly dependent on its length, magnitude of dipole moment of tubulin heterodimer and on viscosity of the environment.
In addition the effective dipole moment of tubulin heterodimer is dependent on the angle of rotation between the vector of the electric field and dipole moment.
The key role in microtubule absorption is the calculation of the relaxation time. We used several techniques to calculation.
We found that permittivity of the environment is affected by presence of proteins, and it is related to the protein concentration. Presence of proteins in aqueous environment leads to a decreased value of the real part of complex permittivity in whole range of measured frequencies (0.2 - 50 GHz) and to an increase of the imaginary part due to a complex dispersion process in proteins.

Key words:

cytoskeleton, microtubules, microwave absorption, protein dielectric properties

Anotácia

Dôvod: Cielom tejto práce bola teoretická štúdia problematiky frekvenčnej závislosti permitivity roztokov vody a proteínov spolu s popisom elektromagnetických vlasností mikrotubulov.

Metódy: Na základe teoretickej štúdie elektromagnetických vlasností proteínov bola vykonaná parametrická analýza absorbcie mikrotubulov. Hlavné parametre absorpcie mikrotubulov boli stanovené za použitia molekulárnych a fyzickálnych prístupov. Boli preskúmané základné vlasnosti proteínov spolu s ich vplyvom na komplexnú permitivitu vo vodnom prostredí. Komplexná permitivita proteínov v roztoku bola experimentálne overená použitím metódy merania permitivity s koaxiálnou sondou a vektorovým analyzátorom od firmy Agilent.

Výsledky a záver: Výpočty ukázali, že absorbčné vlastnosti mikrotubulu sú predovšetkým závislé na jeho dĺžke, veľkosti dipólového momentu jeho základnej stavebnej jednotky heterodiméru tubulínu a na viskozite prostredia. Absorpcia mikrotubulu je taktiež závislá na jeho polohe, rotácii voči dopadajúcej elektromagnetickej vlne.
Výsledky parametrickej analýzy absorbcie mikrotubulov preukázali obtiažnosť experimentálneho overenia ich absorbcie. Hodnoty absorbcie i pri relatívne vysokej koncentrácii vo vodnom roztoku, sú príliš nízke v porovnaní s absorbciou samotného vodného prostredia.
V druhej časti práce boli skúmané vlastnosti proteínov vo vodnom prostredí. Zistili sme, že prítomnosť proteínov ovplyvňuje permittivitu prostredia. Prítomnosť proteínu v roztoku vedie k zníženiu hodnoty reálnej časti komplexnej permitivity v celom rozsahu meraných frekvencií (0.2 - 50 GHz) a ďalej vedie k nárastu imaginárnej časti permitivity v oblasti nižších frekvencií v dôsledku rozptylových procesov spetých s proteínami.

Klúčové slová:

cytoskeleton, mikrotubul, mikrovlnná absorbcia, dielektrické vlastnosti proteínov

Notation and Constants

α	Attenuation factor of the environment	cm^{-1}
β	Force for unit of amplitude	N
δ	Loss angle	-
ΔR	Thickness of the slip layer	m
η_d	Dynamic viscosity of the environment	Pa.s
η_k	Kinematic viscosity of the environment	Pa.s
Γ	Total width	Hz
γ_0	Dumping constant	–
Γ_a	Absorption width	Hz
Γ_s	Emission width	Hz
Γ_{load}	Losses caused by conjugate mismatching	-
λ	Wavelength of the incident radiation	m
μ	Permeability of a specific medium	$H.m^{-1}$
μ_0	Permeability of a vacuum	$H.m^{-1}$
μ_r	Relative Permeability	–
∇	Gradient operator	-
ν_r	Resonant frequency	Hz
ω	Angular frequency	$rad.s^{-1}$
ω_0	Radial frequency of the oscillator	$rad.s^{-1}$
ρ	Protein density	$kg.m^3$
ρ_{ch}	Total charge density	$C.m^{-1}$
ρ_{env}	Environment density	$kg.m^3$
σ_a	Absorption cross-section	cm^2
σ_{ef}	Total effective conductivity	$S.m^{-1}$
τ	Relaxation time	s
ε	Permittivity of a specific medium	$F.m^{-1}$

ε''	Imaginary part of complex permittivity	-
ε'	Real part of complex permittivity	-
ε^*	Complex permittivity	-
ε_p''	Imaginary part of complex permittivity	–
ε_p'	Real part of complex permittivity	–
ε_r	Relative permittivity of the environment	–
ε_r''	Imaginary part of relative complex permittivity	-
ε_r'	Real part of relative complex permittivity	-
ε_0	Permittivity of free space	$\mathrm{F.m^{-1}}$
ε_∞	Optical permittivity	-
ε_s	Static permittivity at 0 Hz	-
φ	Electric potential	V
$\vec{A}$	Work	J
$\vec{B}$	Magnetic field	T
$\vec{D_T}$	Torque	N.m
$\vec{D}$	Electric displacement field	$\mathrm{C.m^{-2}}$
$\vec{d}$	Displacement vector pointing from the negative charge to the positive charge	-
$\vec{E}$	Electric field	$\mathrm{V.m^{-1}}$
$\vec{F}$	Force acting on a dipole	N
$\vec{H}$	Magnetic field	$\mathrm{A.m^{-1}}$
$\vec{J}$	Current density	$\mathrm{A.m^{-2}}$
$\vec{p}$	Electric dipole moment	C.m
$\vec{r}$	Unit vector	-
$\vec{S}$	Poynting vector	$\mathrm{W.m^{-2}}$
a	Amplitude of the oscillation	-
c	Speed of electromagnetic wave in the environment	$\mathrm{m.s^{-1}}$
F_d	Retarding force	N

f_e	Force elastic constant	N
F_v	Viscous force	N
G	Shear modulus	Pa
J	Current density	$\mathrm{A.m^{-2}}$
k	Boltzmann constant	$\mathrm{J.K^{-1}}$
L	Microtubule length	m
l	Dipole length	m
m	Mass	kg
P	Power radiated by an oscillating dipole	W
P_a	Power absorbed by the system	dB
P_r	Power delivered to the receiving load	W
P_ϑ	Power absorbed by water	dB
p_ϑ	Power converted into heat	W
q	Electric charge	C
q_i	Intrinsic quantum yield	–
r	Microtubule radius	m
R_A	Input resistance	Ω
R_L	Load resistance	Ω
R_m	Inner diameter of the microtubule	m
R_{m0}	Outer diameter of the microtubule	m
r_m	Radius of the molecule	m
R_{ohm}	Ohmic resistance	Ω
R_{rad}	Radiated resistance	Ω
Si	Microtubule area surface	$\mathrm{m^2}$
T	Temperature	K
u	Axial component of the velocity	–
V	Load voltage	V

v_a	Velocity of the acoustic wave in microtubule	$\mathrm{m.s}^{-1}$
V_m	Volume of the molecule	m^3
W	Energy	J
w_o	Energy of the oscillator	J
Y	Characteristic admittance of a specific medium	S
Z_A	Input impedance	Ω
Z_A^*	Input impedance (Complex conjugate part)	Ω
Z_L	Load impedance	Ω
I	Incident power flux	$W.m^{-2}$

Acknowledgements

Na tomto mieste by som rád poďakoval vedúcemu diplomovej práce Ing. Ladislavovi Opplovi, PhD., za cenné informácie a rady ohľadom vypracovania diplomovej práce.
Ďalej by som rád poďakoval konzultantovi Ing. Michalovi Cifrovi, Ph.D., za vytvorenie ideálnych pracovných podmienok, ďalej za hodnotné a vecné rady a pripomienky k tématu a taktiež za dobré nasmerovanie mojej životnej cesty.
Taktiež ďakujem Ing. Danielovi Havelkovi za jeho podnetné pripomienky a syntaxiu sadzobného programu Tex.

List of Figures

List of Tables

Contents

Introduction

Living systems, including the human body, consist of such closely interrelated elements that no single element can be fully appreciated in isolation from the others. The unity of living systems is coordinated by many levels of interrelationship. However, to learn about biological systems, we must examine on small portion of a living system at a time. All cells use the same molecular building blocks, similar methods for the storage, maintenance, and expression of genetic information and similar processes of energy metabolism. One of the most important roles in living organism is cell communication. The known form of communication and interaction between cells and between cell and their surrounding environment includes chemical or electrical signals. Basic forms of communication are through hormones, local mediators and through neuronal signaling.

Chemical and electrical interactions within and between cells are well known and well established. On the other hand our knowledge of cellular interactions through other physical fields is limited. One of the probable candidates for another form of cell interactions and communication could by communication through electromagnetic fields.

Due to electrical polar structure of tubulin heterodimer which is the fundamental building block of microtubule, microtubule became one of the candidates for this form of communication. This thesis deals with fundamental biological characterization and calculation of power absorbed by microtubule based on the absorption of dipole antenna and the absorption of electromagnetic radiation by the resonant system.

Second part of the thesis focused on protein structure and its influence on dielectric properties of the aqueous environment. It describes three main processes which play main role in dielectric properties of protein in such environment. At the end we present experimental results of permittivity measurement, and compare them with obtained theoretical knowledge.

1 Cell

All living organisms are composed of cells, small membrane-bounded units filled with concentrated aqueous chemical compounds and fitted with an extraordinary ability to create copies of themselves to grow and divide. The cell is the basic unit of life, which may be the universal answer to the question of what life is and how it works [2]. The largest group of cells is the one containing nucleus (eukaryotic). All complex multicellular organisms including plants, animals and fungi are composed of eukaryotic cells. Example of a eukaryotic cell is shown in Figure 1. A complex system of the cell may by described on the bases of

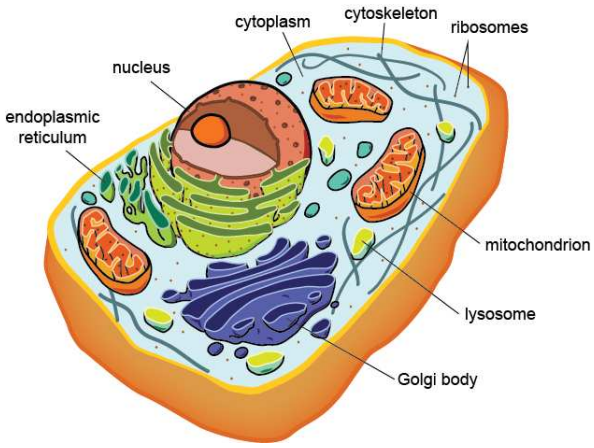

Fig. 1: Example of a Eukaryotic cell [2].

subunits called organelles. The most important organelle is a nucleus. The nucleus is enclosed by two membranes, which formes nuclear core, and contains a very long polymers of DNA with genetic organic code. Another organelle is a mitochondria, which is one of the most spectacular organelle in the cytoplasm and it is present practically in all eukaryotic cells [2]. Other components are ribosomes and a Golgi body emerging from the endoplasmic reticulum. The Golgi is composed of stacks of membrane-bound structures known as cisternae. Each cisterna is comprised of a flat, membrane enclosed disc that includes special Golgi enzymes which modify or help modify cargo proteins that travel through it. Cytoskeleton is the most interesting part of a cell and it is responsible for a formation of a cell.

1.1 Cytoskeleton

The ability of eukaryotic cells holds all parts of their bodies, assuming all sorts of shapes and performing coordinated movements depend on cytoskeleton [2]. In fact, the cytoskeleton can a be very dynamic structure, with components capable of reorganization in less than a minute, or it can be stable for hours at a time [27]. The cytoskeleton is composed of a complex protein fiber network which is situated in the cytoplasm, forming a three-dimensional network inside the cell. Network is made of three types of protein fibers: *intermediate filaments, microtubules and actin filaments*, shown in Figure 2. Each filament system is composed of a polymer created from assembled subunits. Subunits are responsible for filament regulation, and they are also responsible for filament assembly and disassembly, giving the cell flexibility

to create different structures as needed. The cytoskeleton is also connected to the transport-allowing proteins through the cell membrane. It enables transport of molecules and protein structures, receives signals from environment through the cell membrane proteins and plays an important role in a cell growth [27].

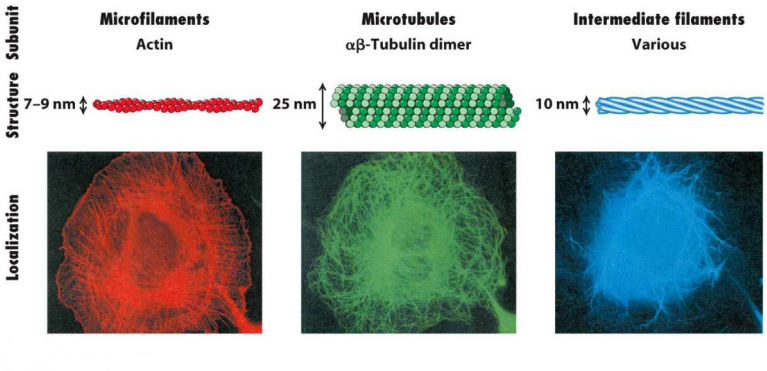

Fig. 2: Protein fibers located in Cytoskeleton [2].

1.1.1 Intermediate filament

Intermediate filaments are fibers with diameter of about 10 nm, created from different kinds of proteins as lamin and creatin. These tissue-specific filament structures serves in number of different ways, including structural support of the nuclear membrane and they provide structural integrity of cells and tissues. They are also different from other protein fibers located in a cytoskeleton because there are no motor proteins that use intermediate filaments as tracks [2].

1.1.2 Microfilaments

Microfilaments are polymers of *actin* protein organized into functional bundles and networks by actin-binding proteins. Microfilaments are especially important in the plasma membrane organization [27]. Actin, as a basic protein unit of microfilaments, exist as a globular monomer called G- actin and as filament polymer called F- actin (see Figure 3). It is a flexible structure with a diameter of 7 - 9 nm. These linear polymers of actin subunits are flexible and relatively strong, resisting buckling by multi-piconewton compressive forces and a filament fracture by nanonewton tensile forces. Their distribution is in the whole cell with the highest concentration in the cortex beneath the plasma membrane [27].

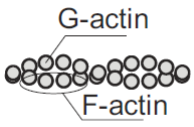

Fig. 3: Actin fiber [12].

1.1.3 Microtubules

A microtubule, found in almost every living system is formed of tubulin subunits, which are arranged in a cylindrical tube structure with an outer diameter of about 25 nm and the inner diameter of about 15 nm. Varying in length from a fraction of a micrometer to hundreds of micrometers, microtubules are much stiffer than either actin filaments or intermediate filaments [2]. The constitutive behavior of cytoskeleton filaments can be integrated into structure based micromechanical models of the entire cell to predict the mechanical response of the combined network in the cytoplasm.

1.2 Microtubules structure and biological function

1.2.1 Microtubule Functions

Cytoplasmic microtubules are responsible for a variety of functions. They maintain axons of nerve cells in mammalian cells. Some migrating mammalian cells require cytoplasmic microtubules to maintain their polarized shape. Cytoplasmic microtubules form the mitotic and meiotic spindles that are essential for the movement of chromosomes during mitosis and meiosis. Cytoplasmic microtubules also contribute to the spatial disposition and directional movement of vesicles and other organelles by providing an organized system of fibres to guide the movement.

Microtubules in eukaryotic cells can be classified into two general groups; axonemal groups and cytoplasmic microtubules. The first group, axonemal microtubules, includes the highly organized stable microtubules found in specific structures associated with cell movement; cilia, flagella and the basal bodies to which these appendages are attached [27]. The central shaft or axoneme of a cilium or flagellum consists of a highly ordered bundle of axonemal microtubules. The second group is the more loosely organized, dynamic network of cytoplasmic microtubules. The second group of microtubules was not recognized until the early 1960s [27].

1.2.2 Microtubule Structure and Organization

As mentioned above, microtubules are basic organizational structure of the cytoskeleton and the whole cell. The outer diameter of a microtubule is about 25 nm while the inner diameter is about 12 nm. Microtubules are highly polar (chemically and electrically) and dynamic deformable structures. They are mostly composed of 13 protofilaments, which are built from blocks of tubulin protein. In rare cases, singlet microtubules contain more or fewer protofilaments; for example, certain microtubules in the neurons of nematode worm contain from 11 to 15 protofilaments [2]. Tubulin isolated in a clean form is composed of subunits called α - tubulin and β - tubulin, each with a molecular weight of about 55,000 Dalton [27]. Genomic analysis revealed the presence of these tubulin units in all analyzed eukaryotic cells. Individual protofilaments are formed by tubulin heterodimers. Tubulin heterodimer and protofilament are shown in Figure 5. Microtubule is shown in Figure 6. Individual α- and β - tubulin molecules have diameters of about 4 - 5 nm. α- and β-tubulin molecules have nearly identical three-dimensional structures [34]. Each tubulin subunit binds two molecules of GTP (Guano-

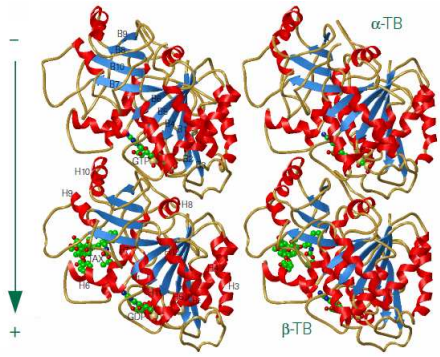

Fig. 4: Dimer consist of α and β - tubulin with GTP, GDP molecules [34].

sine - 5' - triphosphate) (Figure 4). One GTP - binding site, located in α - tubulin, binds GTP irreversibly and does not hydrolyze it, whereas the second site, located on β - tubulin, binds GTP reversibly and hydrolyzes it to GDP (Guanosine - 5'-diphosphate). In a microtubule, lateral and longitudinal interactions between tubulin subunits are responsible for maintaining the tubular shape. The polarity of MT [1] structure arising from the head-to-tail arrangement of the exposed α- and β-tubulin dimers in a protofilament. Microtubules have (+) and (-) end [27] as is shown in Figure 6. The small difference between the α and β - monomers allows the existence of different lattice structures. At the polymerization state, before hydrolysis

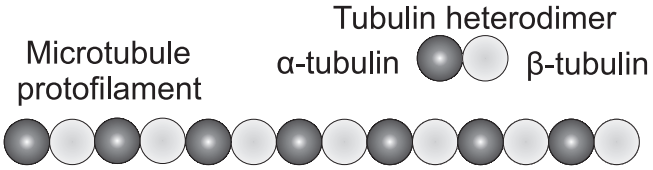

Fig. 5: Tubulin heterodimer and protofilament.

occurs, dimers with GTP molecule are added at the (+) end of the microtubule. That effect leads to the subsequent conversion of GTP to GDP molecule. Thanks to strong GTP binding the MT is stabilized. However, chemical processes occur stochastically, so tubulin at the free end is occasionally hydrolyzed to GDP, what has the effect of tubulin bonds and lead to microtubule disintegration. This process of growth and dynamic instability is described in the following Subsection 1.2.4.

1.2.3 Lattice Structure

There can by only two types of bonds between two tubulin units in the protofilament (between α and β subunits from different tubulin heterodimers). Unlike tubulin bonds in heterodimer, bonds between protofilaments can be created from same subunits ($\alpha-\alpha$ $\beta-\beta$, this is B-lattice) or between different subunits ($\alpha-$ and β, A-lattice (Figure 7)). For the commonly accepted model, moving around the microtubule, in a left-handed sense, protofilaments of the A lattice have a vertical shift of 4.9 nm upwards relative to their neighbors, in the B lattice, this offset is only 0.92 nm [22]. This change results in a *seam* structural discontinuity

[1] MT - microtubule

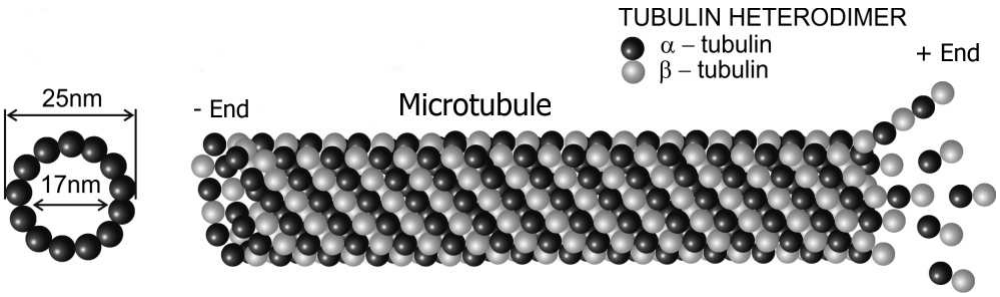

Fig. 6: Microtubule [11].

in the B lattice. The seam implies a neighboring interaction ($\alpha - \beta$) that differs from the majority of the lateral interactions ($\alpha - \alpha$ and $\beta - \beta$) [3].

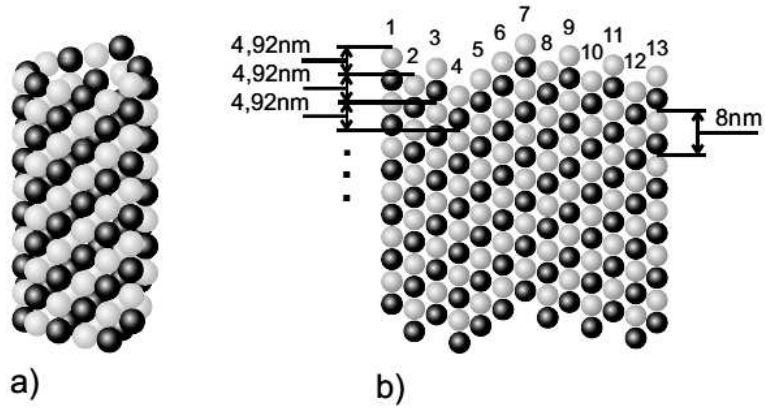

Fig. 7: a) MT composed of 13 protofilaments (lattice A). b) Lattice structure [22].

1.2.4 Growth and Microtubule Dynamics

With the identification of tubulin as the major structural component of microtubules, antibodies of tubulin were generated and used in immunofluorescence microscopy to localize microtubules in cells [2]. This approach coupled with the description of microtubules is assembled from specific sites to generate many different types of organization. The nucleation phase of microtubule assembly is such an unfavorable reaction that spontaneous nucleation does not play a significant role in microtubule assembly in vivo. Growth of all microtubules is controlled by the structure called MTOC [2]. The MTOC in animal cells is a centrosome structure. In most cases, (-) end of MT is bound to centrosome, while (+) end grows towards the cytoskeleton. Presence of γ - tubulin plays an important role in growth also, because it enable to create different shapes on the centrosome surface which are responsible of MT growth [27]. An example of the centrosome is shown in Figure 8. The centrosome is the main MTOC in animal cells, the centrosome is generally located near the nucleus, producing an array of microtubules with their (+) ends radiating toward the cell periphery. This radial display

[2]MTOC - microtubule - organizing center

provides tracks for microtubule-based motor proteins to organize and transport membrane-bound compartments, such as those comprising the secretory and endocytic pathways. As

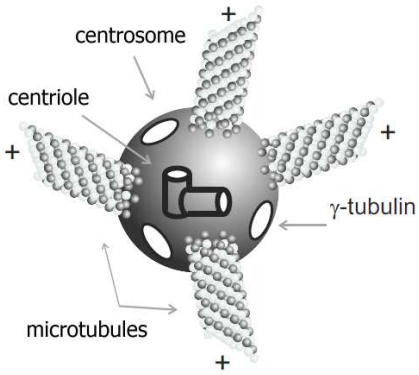

Fig. 8: Centrosome [11].

mentioned above, the assembly dynamic is stochastic for every individual MT. The rate of shortening is about ten times the rate of growth and a stochastic model may be developed for studying individual growth. The probability of a single MT nucleating, growing, shortening and so on, depends on the local concentration of tubulin with GTP bound, tubulin with GDP bound and on other molecules relevant to the assembly process which are found within the cytoplasm [27]. Thus the dynamic life of a microtubule end is determined by the rate of depolymerization, and the frequency of rescues. Since the (-) ends of the microtubules in animal cells are generally anchored on an MTOC, this dynamic nature is most relevant to the (+) end of the microtubule. Many theoretical models [10] have successfully reproduced the single MT growth behavior. Microtubule dynamic instability is illustrated in Figure 9.

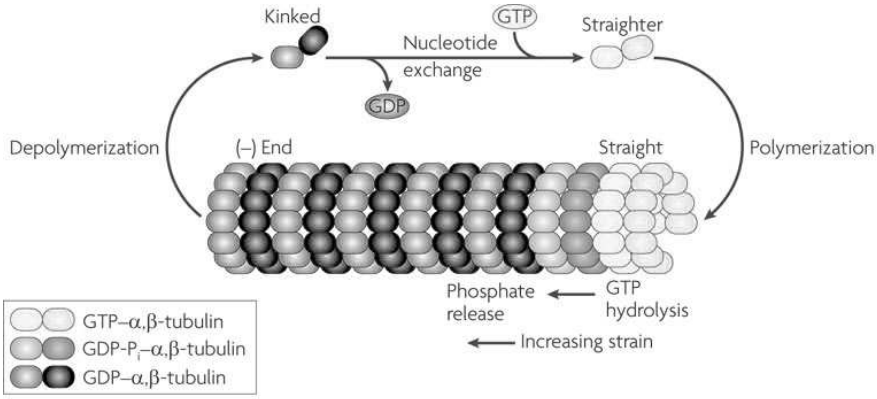

Fig. 9: Microtubule dynamic instability cycle.

1.2.5 Regulation of Microtubule Structure and Dynamics

The wall of MTs is built of $\alpha\beta$ - tubulin dimers, an highly purified $\alpha\beta$ - tubulin will assemble in vitro into microtubules. But assembly of microtubules in vitro can be greatly enhanced by the presence of stabilizing microtubule - associated proteins (MAPs) [27]. Stabilizing MAPs protein represents just one class of the protein that interacts with tubulin in microtubules, other classes destabilize microtubules, or modify their growth properties. Among the best studied are Tau (τ) family of proteins, which includes τ itself, and proteins called MAP1, MAP2 and MAP4 [2] (Figure 10). Tau and MAP2 are neuronal proteins, while MAP4 is defined by other cell types and is generally not present in neurons. Tau proteins are believed

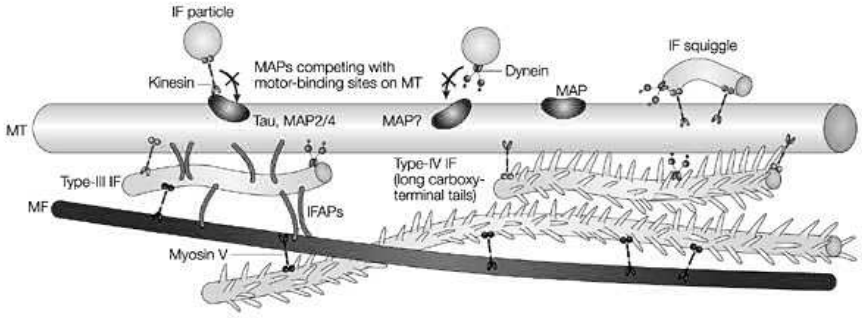

Fig. 10: Microtubule with side-binding proteins MAP.

to stabilize microtubules and also to act as spacers between them. MAP2 is found only in dendrites of neurons, where it forms fibrous cross-bridges between microtubules and links microtubules to intermediate filaments. Each of the MAPs seems to serve a similar role but is localized in a different cell. MAP1 has two main forms known as MAP1A and MAP1B. MAP1B is predominantly an axonal protein and is found consistently in extending neurites, it is believed to promote the outgrowth of neurites by stimulating MT assembly [10]. MAP1A on the other hand seems to stabilize existing axons and dendrites [10]. The expression of MAP1A is complementary to the expression of MAP1B such that once sufficient assembly has occurred, MAP1A may act to stabilize the MTs. The action of MAP2 is to stimulate MT polymerization and it acts by reducing the critical concentration of required tubulin [27]. It is expressed exclusively in neuronal cells and its high molecular weight form is found only in dendrites. Tau is also localized to neurons, but is almost exclusively found within axons. Interest in this protein has been spurred by the discovery of its association with Alzheimer's disease [10]. The association between MAPs and tubulin may be instrumental in the ordering of dipoles and signal propagation. Although not usually considered in the same context, motor proteins such as kinesin and dynein are another sort of microtubule-associated proteins. Their interaction with tubulin seems to be mechanical only as they walk along the MT lattice transporting goods towards or away from the nucleus [12].

2 Electrodynamic properties of microtubules

Many processes in the cell are connected with charge motion. From Maxwell's equations we know that there is an electric and magnetic field generated by a moving charge. When the charge is changing the speed of its own oscillation, there is a change in the electric field, which leads to an increase of the magnetic field and vice versa. There is such generation of electromagnetic field in the cell, especially during the electrochemical reactions, which result in a very weak EM[3] field at frequencies up to a few tens of Hz [13]. These effects occur only in groups of specialized cells of higher organisms. We will examine the possibility of electromagnetic generation in non-specialized cells. The following subsection shortly describes one of the three processes which may be responsible for this phenomenon (All processes are described in Appendix 8).

2.1 Mechanical vibrations of electrically polar structures

Process which can take place in the cell electrodynamic generation is based on the vibrations of electrically polar biomolecular cellular structures. Vibration frequency depends on the size and structure rigidity [26], as well as on the type of vibration mode. Vibrating modes of biomolecules have been studied by several types of spectroscopy [5]. It is also known that a cell contains either the internal structure of the electrically polar (most proteins are electrically polar), or structures such as membranes, which are electrically polarized to different electric potential on their sides. The basic idea is that metabolic energy produced in specific types of cell structure can provide energy for vibrations of electrically polar molecules. These vibrations can be a source of electromagnetic field. The following text describes the theory of Herbert Fröhlich, who postulated the possibility of electromagnetic field generation in biological systems under certain specific conditions based on electrically polar structure vibrations.

2.1.1 Fröhlich theory

The idea of electromagnetic field generation in biological systems was first presented by theoretical physicist Herbert Fröhlich. This idea was based on the theory which tried to explain the origin and action mechanisms of electromagnetic fields in biological systems. Fröhlich postulated that coherent longitudinal electrically polar vibrations in biological systems are based on a strong electrically polar character of biosystems (cellular membrane was considered). These should be the modes that establish long range correlations in biosystems. Longitudinal modes can be strongly excited since they don't lose energy by radiation. If their frequency is relatively low, energy can be lost by friction. However his model did not include particular cellular structure. The subsequent review of the cytoskeleton, microtubule became another possible source of electromagnetic field in cell. As was described in Subsection 1.2.2 microtubules are composed of a number electrically polar tubulin units. In Subsection 1.2.4, was mentioned that MTs are very dynamic structures with alternating growth period (tubulin polymerization) and reduction period (tubulin depolymerization). This

[3] EM - electro - magnetic

dynamic instability is accompanied by a constant influx of energy from interleaving GTP-rich tubulin heterodimer. Other energy suppliers are likely to be motor proteins moving along microtubules [3] and mitochondria, which replicate the microtubular network.

2.2 Electric dipole moment of microtubule

In the case of an electromagnetic absorption it is important to describe electric properties of microtubules. For this description we used the basic microtubular unit - tubulin heterodimer. For the purpose of MTs analysis as electric system we approximate tubulin heterodimer as electric dipole (Fig. 11). This approximation plays the key role in the electric characterization of the MT. Dipole moment in the simple case of two point charges is given as:

$$\vec{p} = q.\vec{d} \tag{1}$$

where $\vec{d}$ is the displacement vector pointing from the negative charge to the positive charge q. Thus, the electric dipole moment vector $\vec{p}$ points from the negative charge to the positive charge. Charge distribution on tubulin has generally multipolar character and can be measured or be calculated from the molecular calculations [32]. We can use the Equation (1)

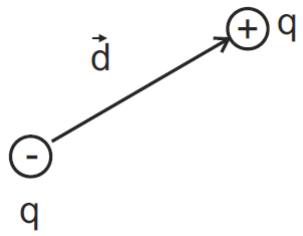

Fig. 11: Dipole moment $\vec{p}$ in the simple case of two point charges.

for the calculation of the electrostatic potential created by the point dipole. Electrostatic potential due to dipole moment can be written as [44]:

$$\varphi = \frac{1}{4\pi\varepsilon_0}\frac{q\vec{d}\cos\theta}{r^2} = \frac{1}{4\pi\varepsilon_0}\frac{\vec{p}.\vec{r}}{r^3} \tag{2}$$

where ε_0 is the permittivity of free space, $\vec{r}$ is a unit vector.
From the Equation (2) we can see that the potential is proportional to the dipole moment. Now we can write equation for an electric field generated by point dipole (in our case molecule of dimer) as [40]:

$$\vec{E} = -\nabla\varphi = \frac{1}{4\pi\varepsilon_0}\left[\frac{3(\vec{p}.\vec{r})\vec{r}}{r^5} - \frac{\vec{p}}{r^3}\right] \tag{3}$$

where $-\nabla\varphi$ is the negative gradient of the scalar electric potential.
If we put this dipole into the outer homogenous field ($E = const.$) there will be no force acting on the dipole, there will by only moment of a force (torque) [15]:

$$\vec{D_T} = \vec{p} \times \vec{E} \tag{4}$$

The torque tends to align the dipole with the field, and thus it is decreasing an angle θ between dipole direction and direction of the field. The work done by the moment of a force during the rotation can be written as [15]:

$$A = \int_{\pi/2}^{\alpha} \vec{D_T}\, d\alpha = \int_{\pi/2}^{\alpha} \vec{p}\vec{E} \sin\alpha\, d\alpha \;=\; -\vec{p}\vec{E}\cos\alpha \tag{5}$$

Dipole will obtain an energy which depends on the orientation towards the direction of the field. This energy is equal to [44]:

$$W \;=\; -\vec{p}.\vec{E} \tag{6}$$

In inhomogeneous field there will be some non-zero force which will be acting on a dipole. In general case we can obtain this force from the Equation (6):

$$\vec{F} = -\nabla W = \nabla(\vec{p}.\vec{E}) = (\vec{p}\nabla)\vec{E} \tag{7}$$

Generally we can say that, the electric dipole (in our case tubulin heterodimer) oriented parallel to field direction will be drawn to area with greater electric intensity, dipole oriented non - parallel will be forced out of this area. Free oriented dipole in an inhomogeneous field will be initially rotated by the action of torque to field direction and then will be dragged to an area with greater intensity. This description of dipole behavior is very simplified. As was stated in Subchapter 1.2.2 microtubule consists of several tubulin heterodimers which interact together. Moreover, the cell itself is a complex structure consisting of many parts that can influence this process. One example is a dependence between electric dipole moment and charge (see Equation (1)). In normal physiological conditions (pH = 7.4) microtubules are negatively charged [29] thanks to presence of C - termini domain. Detailed description between pH and dipole moment is shown in the work of Tuszynski [45]. First calculations of dipole moments in complex molecules was performed by Nogales in 1998 [33] by electron crystallography. Mershin et al. [29] calculated dipole moment independently for α and β - monomer as $|\vec{p}_\alpha| = 552\,\mathrm{D}$ and $|\vec{p}_\beta| = 1193\,\mathrm{D}$. Dipole moments of individual monomers are not completely parallel, with the superposition we receive $|\vec{p}_{\alpha\beta}| = 1740\,\mathrm{D}$.
Similar value was calculated by Tuszynski et al. in their work [45] (1714 D). Brown in his work [10] described interactions between dipole moments. Dipole moment components are shown in Table 1. We see that dipole moment is primarily oriented radially to the axis of

p_x	337 D
p_y	-1669 D
p_z	198 D

Tab. 1: Calculated dipole moments for individual axes [45].

the MT (Fig. 13). However, there is a small contribution in direction of X axis. Many other factors can influence dipole orientation. In addition, its orientation can be affected by a double layer of polymerized states (Fig. 12). Another factor is the existence of hydrophobic protein capsules containing 2 x 18 unpaired electrons in two potential areas [28].

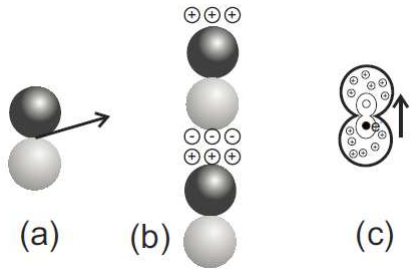

Fig. 12: Contribution to the internal dipole moment: a - the internal dipole moment, b - double layer of polymerized states, c - two hydrophobic pocket containing unpaired electrons.

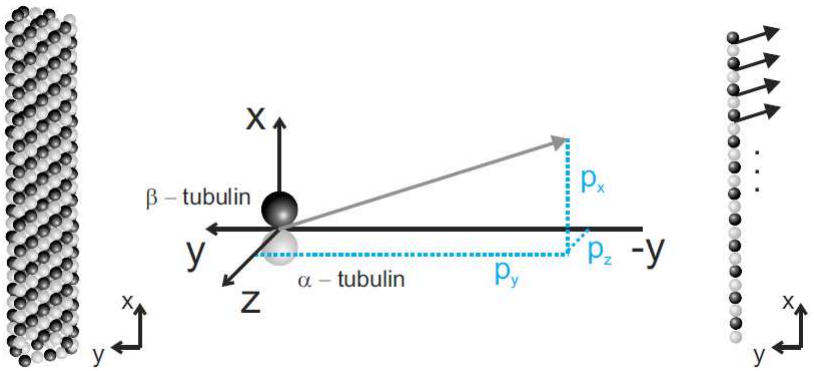

Fig. 13: Dipole moment orientation of tubulin calculated from crystallographic data.

Work by Vassilev et al. [46] is one of the experimental works describes the electromagnetic field effect on microtubules. They investigated effects of electric and magnetic field on MT assembly. The idea was that the voltage gradients generated in the cell may have effect on MT growth. They purified microtubules from rats brains and they investigated effect of electric and magnetic field at constant temperature of 37 °C. After application of electric field with frequency of 10 Hz and 25 mV/cm amplitude they observed parallel compilation of MTs and their common orientation in field direction. The same phenomenon was observed also in magnetic field (0.02 T) application for 10 min. Based on these results they considered that microtubules have tendency to periodically organize in presence of the field. Based on this knowledge they expressed the idea of possible orientation control in cell which can be achieved by the weak electric and magnetic field generated by mitochondrias.
Stracke et al. [42] also analyzed microtubules behavior in electric field. They created parallel positions of MTs by using application of electric field field. They were trying to control there movement through the kinesin-coated surface in desired direction. For nearly ideal physiological conditions (pH 6.8) MTs had tendency to move towards anode with an electrophoretic mobility of approximately 2.6×10^{-4} cm^2/V which corresponded to negative charge of tubulin dimers. Moreover, the results of an experiment indicate that microtubule formation is accompanied by substantial changes in charge distribution within tubulin subunits. It showed that constant electric fields have an impact on MTs orientation and surface gliding (pH 6.8). Another work was trying to explain MT behavior in electric field and determine its dipole

moment was work wrote by Konrad et al. [9]. They investigated microtubules behavior in high-frequency electric field (2.1×10^5 V/m, 200 kHz - 2 MHz). They were trying to determine electric dipole moment from the angular velocity of microtubule tilting the sample under the influence of electric field. Work confirmed that microtubules are affected by this field and if DC field was applied MTs have tendency to orient in field direction.

2.3 Microtubule vibration modes

Mechanical vibrations in microtubules can generate electric field around them. Energy sources for mechanical vibrations were analyzed in many works [37, 12]. Energy delivered to microtubule for these vibrations can be a result of GTP to GDP transformation, second from the energy which is not used by mitochondria but it is radiated as infrared radiation into the environment, and third from motor proteins (dynein, kinesin) movement along microtubule. However the consideration of mechanical oscillations, appeared to be an unrealistic idea for many scientists. Reason being the microtubule environment. As was described in Subchapter 1.1, microtubules are part of cytoskeleton. Cytoskeleton also contains protein fibers and relatively large amount of water, which has viscous gel-like character [2]. This environment, should act as a damping environment to any mechanical vibrations. Even if some oscillations occurs, it should be very quickly subdued by the environment. One of the possible solutions of this problem was presented by Pokorný, who in his work [37] described creation of a structure, which we call bound (or organized) water. His work describes the idea of charge layer created by ions from cytoskeleton [42]. Since the cytosol environment also penetrates MT inside similar situation may occur inside the microtubule (Fig. 14) Layer of ions can inhibit microtubule electrical potential [42]. Static potential is considerably shielded to distance about 1.6 nm. Through hydration, ions are surrounded by water molecules to a distance of 0.4 - 0.5 nm. Charged proteins with significantly bigger size than the ionized atoms can be also present in the ionic layer. Most of the water molecules in the charged layer is not free, but its viscous properties are dependant on hydrated ions. Based on the theory that was postulated in his work [38] some ions can penetrate tubulin structure and act as part of tubulin (as well as molecule of water). He also argues that the ions in cytosol have little mobility, and is therefore a slip between the charged layer and microtubule surface. Therefore,

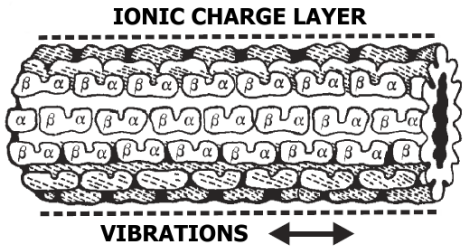

Fig. 14: Schematic representation of MT with ionic charge layer.

the water around microtubule in certain conditions can create the structure, which is often called bound water. Pokorný in his work [38] argues and documents many scientific articles which provide experimental evidence that bound water has a lower emissivity and Brownian

movement, but due to its own structure is also more dense than ordinal water. Therefore organized water is expected to reduce longitudinal vibration damping with comparison to free water, due to the existence of sliding surface along microtubule structure created by this water. The thickness of such water layer may reach up to several μm [12, 37, 22].

Possible mechanical vibrations are associated with microtubule electrodynamic field generation. Spatial distribution of these vibrations from minimum to maximum can be in the order of hundreds nm. Calculations of electrodynamic field approximates to vibration modes which indicate the phase shift between individual dimers in protofilament. If the phase shifts between neighboring dimers are zero (all dimers oscillating in phase) we call this state the base mode. In the event of neighboring dimer oscillating out of phase (phase shift is 180), it is the maximum mode. Mode 1 can be described as half of the microtubule wavelength. Mode 2 as one microtubule wavelength etc. Maximum mode corresponds to the number of heterodimers in protofilament.
The calculation of microtubule electrodynamic field was the main theme for many works, for example Pokorný et al. [39], Cifra et al. [12, 11], Havelka et al. [22, 21].

3 Complex permittivity of proteins in solution

This chapter focuses on an electrical description of proteins in general aqueous solution. The general interaction of an electric field with a dielectric material is described. The polarization effects give insight to cellular mechanisms at a molecular level.

The complex permittivity is a quantity which describes the electrical properties of materials. In case of non-conductors, dielectrics, the complex permittivity describes interaction between the dielectric and the applied external electric field [47]. Measurement of the electromagnetic response of materials at microwave frequencies is important for both fundamental and practical reasons. The dielectric properties of materials give insights into the polarization dynamics on the practical side. Our goal is to explain the phenomena of complex permittivity in protein solutions. The motivation for future experimental work will be the measurement of the permittivity of tubulin in solutions.

3.1 Fundamental of electromagnetic Field

The calculation of electromagnetic field quantities means solving Maxwell's equations which are the basic equations of electrodynamics.

$$\nabla \times \vec{H} = \vec{J} + j\omega\vec{D} = \sigma\vec{E} + j\omega\varepsilon\vec{E} \tag{8}$$

$$\nabla \times \vec{E} = -j\omega\vec{B} = -j\omega\mu\vec{H} \tag{9}$$

$$\nabla \cdot \vec{D} = \nabla \cdot \varepsilon\vec{E} = \rho_{ch} \tag{10}$$

$$\nabla \cdot \vec{B} = \nabla \cdot \mu\vec{H} = 0 \tag{11}$$

where $\vec{H}$ is magnetic field, $\vec{J}$ current density, ω angular frequency, $\vec{D}$ electric displacement field, $\vec{B}$ magnetic field, ρ_{ch} is the total charge density.

3.2 Dielectrics in alternating field

If the dielectric is in the alternating electric field, also the polarization field $\vec{P}$ and electric flux density $\vec{D}$ change periodically in time. But generally the variables $\vec{P}$ and $\vec{D}$ could be phase delayed in respect to the variable $\vec{E}$:

$$E = E_0 \cos \omega t \tag{12}$$

and

$$D = D_0 \cos(\omega t - \delta) = D_1 \cos \omega t + D_2 \sin \omega t \tag{13}$$

where δ is loss angle and D_1 and D_2 are:

$$D_1 = D_0 \cos \delta, \;\; D_2 = D_0 \sin \delta \tag{14}$$

for the most of dielectrics is D_0 directly proportional to E_0 but the ratio $\frac{D_0}{E_0}$ is a frequency dependent in principle. In order to describe these effects we introduce two new frequency dependent variables:

$$\varepsilon^{'} = \frac{D_1}{E_0} = \frac{D_0}{E_1} \cos \delta \tag{15}$$

$$\varepsilon^{''} = \frac{D_2}{E_0} = \frac{D_0}{E_1} \sin \delta \tag{16}$$

which can be joined into one complex quantity, so called a *complex permittivity*

$$\varepsilon^* = \varepsilon^{'} - j\varepsilon^{''} \tag{17}$$

where $\varepsilon^{'}$ is real part and $\varepsilon^{''}$ imaginary part of complex permittivity. If D and E are expressed as complex quantities, the relation between them is simply [47]:

$$D = \varepsilon^* E_0 \exp(j\omega t) \tag{18}$$

The complex permittivity ε^* describes the interaction of an external electric field with protein solution and because of the loss character of protein solution it is a complex quantity. In terms of relative permittivity is relative complex permittivity given as [40]:

$$\frac{\varepsilon^*}{\varepsilon_0} = \varepsilon_c = \varepsilon_r^{'} - j\varepsilon_r^{''} \tag{19}$$

where $\varepsilon_r^{'}$, $\varepsilon_r^{''}$ is real, imaginary part of relative complex permittivity. The real part of complex relative permittivity $\varepsilon_r^{'}$ is a measure of how much energy from an external electric field is stored in a material and the imaginary part of complex relative permittivity $\varepsilon_r^{''}$ (loss factor) is a measure of how dissipative or lossy a material is to an external electric field. The loss factor includes the effects of both dielectric loss and conductivity. Dissipation factor is defined by ratio of imaginary to real part of complex permittivity

$$\tan \delta = \frac{\varepsilon_r^{''}}{\varepsilon_r^{'}} = \frac{1}{Q} = \frac{Energy\, lost\, per\, cycle}{Energy\, stored\, per\, cycle} \tag{20}$$

The loss tangent or $\tan\delta$ is defined as the ratio of the imaginary part of the dielectric constant to the real part. Q is quality factor due to dielectric losses. The loss tangent $\tan\delta$ is called tan delta, tangent loss or dissipation factor. Sometimes the term *quality factor or Q-factor* is used with respect to microwave material, which is the reciprocal of the loss tangent. This term is valid for only small angles of δ when is valid $\tan\delta = \sin\delta = \delta$. It is important to note that complex permittivity is a variable quantity, it changes with frequency, temperature, orientation, mixture, pressure, and molecular structure of a material.

3.3 Dielectric Mechanisms

A material may have several dielectric mechanisms or polarization effects that contribute to its overall permittivity (Figure 15). A dielectric material has an arrangement of electric charge carriers that can be displaced by an electric field. The charges become polarized to compensate for the electric field such that the positive and negative charges move in opposite directions. At the microscopic level, several dielectric mechanisms can contribute to dielectric behavior. Dipole orientation and ionic conduction interact strongly at microwave frequencies. Water molecules, for example, are permanent dipoles, which rotate to follow an alternating

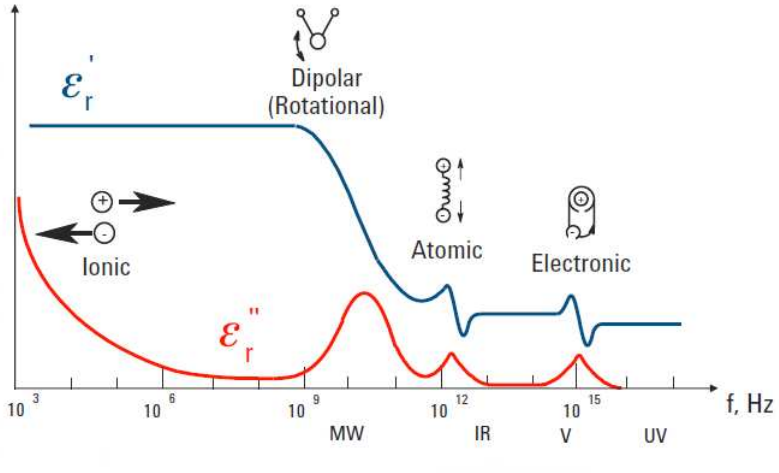

Fig. 15: Frequency response of dielectric mechanisms.

electric field. These mechanisms are quite lossy. Atomic and electronic mechanisms are relatively weak, and usually constant over the microwave region. Each dielectric mechanism has a characteristic "cutoff frequency". As frequency increases, the slow mechanisms drop out in turn, leaving the faster ones to contribute to $\varepsilon_r^{'}$. The loss factor $\varepsilon_r^{''}$ will correspondingly peak at each critical frequency. The magnitude and cutoff frequency of each mechanism is unique for different materials. Water has a strong dipolar effect at low frequencies – but its dielectric constant drops dramatically around 22 GHz.

3.4 Relaxation time

Relaxation time τ is a measure of the mobility of the molecules (dipoles) that exist in a material. It is the time required for a displaced system aligned in an electric field to return

to $1/e$ of its random equilibrium value. It is frequently defined as the time which is required for the polarization to decrease to $1/e$ of the original value. Liquid and solid materials have molecules that are in a condensed state with limited freedom to move when an electric field is applied. Constant collisions cause internal friction so that the molecules turn slowly and exponentially approach the final state of orientation polarization with relaxation time constant τ. When the field is switched off, the sequence is reversed and random distribution is restored with the same time constant. The relaxation frequency f_c is inversely related to relaxation time:

$$\tau = \frac{1}{\omega_c} = \frac{1}{2\pi f_c} \tag{21}$$

At frequencies below relaxation the alternating electric field is slow enough that the dipoles are able to keep pace with the field variations. Because the polarization is able to develop fully, the loss ($\varepsilon_r^{''}$) is directly proportional to the frequency (Figure 16a). As the frequency increases, $\varepsilon_r^{''}$ continues to increase but the storage ($\varepsilon_r^{'}$) begins to decrease due to the phase lag between the dipole alignment and the electric field. Above the relaxation frequency both $\varepsilon_r^{''}$ and $\varepsilon_r^{'}$ drop off as the electric field is too fast to influence the dipole rotation and the orientation polarization disappears.

3.5 Debye-Strogyn dielectrics

The classical approach to the treatment of permanent dipoles in liquids and in solutions of polar molecules in non-polar solvents is to consider their behavior in alternating fields as arising from the rotation of a spherical dipole in a viscous medium dominated by friction. Debye working on electrolytes deduced the well known equation:

$$\varepsilon^* = \varepsilon_r^{'} - j\varepsilon_r^{''} = \varepsilon_\infty + \frac{\varepsilon_s - \varepsilon_\infty}{1 + j\omega\tau} \tag{22}$$

where ε_∞ is the optical permittivity at very high frequencies and ε_s is the static permittivity at 0 Hz. Separating the real and imaginary parts and rearranging we obtain:

$$\varepsilon^{'} = \varepsilon_\infty + \frac{\varepsilon_s - \varepsilon_\infty}{1 + \omega^2\tau^2} \tag{23}$$

$$\varepsilon^{''} = \frac{(\varepsilon_s - \varepsilon_\infty)\omega\tau}{1 + \omega^2\tau^2} \tag{24}$$

These quantities are plotted in Fig. 16a as functions of frequency f. It should be noted that the maximum value for the dielectric loss occurs at $\ln\omega\tau = 0$ where the critical angular frequency is given by $\omega_c = 1/\tau$. In our model of water and protein we also used the another Debye form of equation which was used by Stogryn [41] for calculating the dielectric constant of saline water:

$$\varepsilon^* = \varepsilon_\infty + \frac{\varepsilon_s - \varepsilon_\infty}{1 + j\omega\tau} + j\frac{\sigma}{2\pi\varepsilon_0 f} \tag{25}$$

which includes solution conductivity (σ) for imaginary part of complex permittivity.

3.6 Cole-Cole diagram

The data provided by dielectric measurements can be presented in different ways. One classical representation is in plotting the real and imaginary parts of the permittivity as functions of frequency f. The disadvantage, however, is that these two plots are then presented independently of each other while their frequency behaviors are linked through the general theoretical considerations. Cole-Cole diagram is, to some extent, similar to the Smith chart. A material that has a single relaxation frequency as exhibited by the Debye relation will appear as a semicircle with its center lying on the horizontal $\varepsilon_r'' = 0$ axis and the peak of the loss factor occurring at $1/\tau$. A material with multiple relaxation frequencies will be a semicircle (symmetric distribution) or an arc (nonsymmetrical distribution) with its center lying below the horizontal $\varepsilon_r'' = 0$ axis. The curve in Figure 16b is a half circle with its center on the x-axis and its radius $\frac{\varepsilon_s - \varepsilon_\infty}{2}$. The maximum imaginary part of the dielectric constant ε'_{max} will be equal to the radius. The frequency moves counter clockwise on the curve. Debye permittivity of water was calculated from Equation (22), Strogyn from Equation (25).

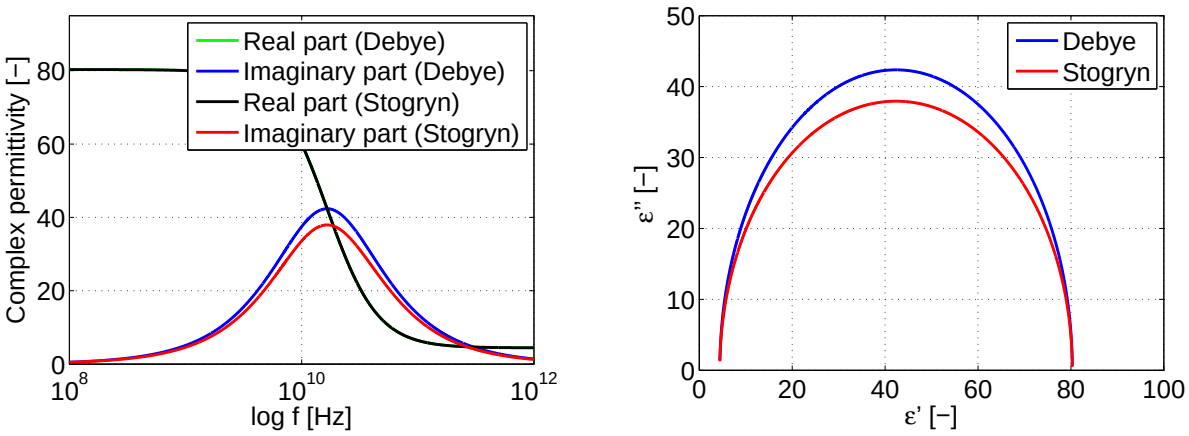

(a) Debye-Strogyn relaxation of distilled water at 296.15 K.

(b) Debye-Strogyn Cole-Cole diagram of distilled water at 296.15 K.

Fig. 16: Relaxation and Cole-Cole diagram of distilled water at 296.15 K.

3.7 Dielectric properties of proteins

Globule protein is one of the most important materials in biology. It has a lot of biological functions in living materials. For example, the enzyme works as a catalyst of hydrolysis, oxidation and reduction [2]. In the living materials the protein molecules are surrounded by water in most cases. Therefore it is of particular interest to investigate the water structure around the protein. High resolution x-ray and neutron diffraction measurements in the crystal phase have made clear that there are peculiar water molecules correlating strongly with the globule protein [14]. It is suggested that the water molecules attach the oxygen, nitrogen, and polar groups on the globule protein surface through hydrogen bonding [31]. This bound water is thought to give an important influence on the functions of protein. In the case of trypsin of hydrolase, such water molecules construct a network with polar groups,

which maintains the shape of active sire, and stabilizes the protein structure [31]. Studying dielectric relaxation in one of the ways of obtaining useful information on the physicochemical properties of proteins in solution. Ignoring low-frequency processes of less interest, solutions of proteins show fairly simple dielectric spectra with two major dispersion/loss regimes center near 10 MHz (so called β - relaxation) and 10 GHz (γ - relaxation) and a minor contribution near 100 MHz (δ - relaxation) [25]. Phenomenologically, the β- and γ - process are usually rationalized by protein tumbling and reorientation of bulk water, respectively. The δ - process is thought to arise either from the motions of protein - bound waters, from protein - water interactions, and/or from motions of polar side groups of protein [25].
However, it has been thought to be difficult to measure the dielectric relaxation of globule protein in aqueous solution, since the solvent has usually a large dielectric constant and relaxation strength of the bound water is thought to be too small to be observed distinctively. We made permittivity measurement of BSA protein in solution with high concentrations. The experimental part with methodology of protein measurement is described in Subchapter 7.3.

For modeling of water permittivity we used common Equation (23) for real part, Equation (24) for imaginary part which was described in previous Subchapter 3.5 together with comparison with Stogryn model defined by Equation (25). Then we tried to applied this model on protein permittivity (see Figure 50) in Subchapter 7.3.4. Next model was based on Debye relaxation equation. The Debye relaxation equation describes permittivity response of polar liquids within the microwave regime and is given by [6]:

$$e^*(\omega) = \varepsilon_\infty + \sum_{j=1}^{n} \frac{\varepsilon_j - \varepsilon_{j+1}}{1 + i\omega\tau_j} + \frac{i\sigma}{\omega\varepsilon_0} \tag{26}$$

where ε_j and ε_{j+1} are the permittivities before and after a relaxation process τ_j. For protein relaxation time we used the equation (Approximation based for overall rotation of spherical molecule in a viscous medium [31]):

$$\tau = \frac{4\pi {r_m}^3}{kT}\eta = \frac{3V_m}{kT}\eta \tag{27}$$

where r_m is the radius of molecule, V_m is its volume, T is temperature, k Boltzmann constant and η is solvent viscosity. It is thus indicated that the relaxation time is proportional to the molecular weight, if the globule protein is assumed to be a sphere [31]. We applied Equation (26) to measured protein permittivity. The result is shown in Figure 51.

My procedure for relaxation time calculation of BSA protein was as follows. I used bovine serum albumin molecular dimensions ($40 \times 40 \times 140$ Å) and calculated its volume V_m. Then the Boltzmann constant and temperature of 296,15 K was used. For viscosity η I used the standard dynamic viscosity of water, which gives us the final relaxation time of BSA protein molecule $\tau = 164$ ns (experimental results show that relaxation time of BSA protein is in the region of $\tau = 200$ ns [20]). Permittivities ε, ε_j were taken from experimental results with BSA concentrations and from theoretical values of water.

4 Absorption of microtubules

Knowledge of the MT absorption is one of the key characteristics that will enable us to determine his own quality factor (Q). Specifying of quality factor is a key for consideration of any MT interaction with EM field. We used two basic approaches for calculations. The first idea was to replace MT which we considered to be an electrically polar structure with a dipole antenna. In this approximation we considered that the absorption is equivalent to power delivered to the load (P_r). Based on this model, we made an analysis in Subsection 4.1. The second proposal was to approximate MT as resonant system and its interaction with electromagnetic wave (Subsection 4.2).

4.1 Microtubule as dipole antenna

In first step of dipole antenna approximation I used the circuit equivalent of transmitting antenna 17.

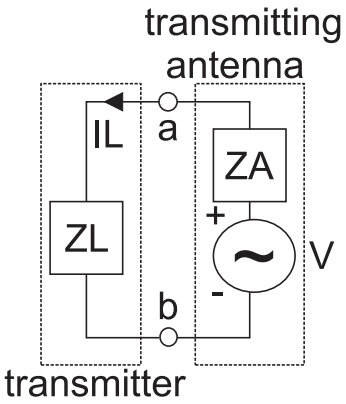

Fig. 17: Circuit equivalents of transmitting antennas.

Power delivered to the receiving load is equal to [30]:

$$P_r = \frac{1}{2}|\ I_L\ |^2 R_L = \frac{1}{2}\frac{|\ V\ |^2 R_L}{|\ Z_L + Z_A\ |^2} \tag{28}$$

where V is load voltage, Z_L load impedance ($Z_L = R_L + jX_L$), R_L load resistance, Z_A input impedance of the antenna ($Z_A = R_A + jX_A$). Input resistance of the antenna include losses $R_A = R_{rad} + R_{ohm}$ where R_{rad} is radiation resistance and R_{ohm} is ohmic resistance.

4.1.1 State with conjugate matching condition

For this calculation we used conjugate matching condition $Z_L = Z_A^*$. Power delivered to the receiving load can be now calculated as:

$$P_r = \frac{1}{2}|\ I_L\ |^2 R_L = \frac{1}{2}\frac{V^2|\ R_L\ |}{|\ Z_L + Z_A\ |^2} \approx P_{r,max} = \frac{|\ V\ |^2}{8R_A} \tag{29}$$

Input resistance of an antenna is equal to $R_A = R_{rad}+R_{ohm}$. For R_{rad} I will use the formula for dipole radiation resistance (valid for very short length of an antenna l) $R_{rad} = 80\left(\frac{\pi l}{\lambda}\right)^2$ [30]. Im expressing load voltage as $V = El$ where l is dipole length. After substituting into the Equation (29) I will get:

$$P_r = \frac{\mid V \mid^2}{8R_A} = \frac{E^2\lambda^2}{640\pi^2 + R_{ohm}} \tag{30}$$

In an ideal case $R_{ohm} = 0$ and after substituting into (30) the final solution can be expressed as:

$$P_r = \frac{E^2\lambda^2}{640\pi^2} \tag{31}$$

where λ is wavelength of the incident radiation. In ideal case is absorption of dipole antenna expressed by equivalent of power received to the load which is proportional to incident radiation wavelength and electric field.

4.1.2 State without conjugate matching condition

For general relationship I consider circuit 17 without impedance matching. I consider also non-zero ohmic losses R_{ohm}. Power delivered to the receiving load can be now calculated as [23]:

$$P_r \; = \; P_{r,max}(1 - \mid \Gamma_{load} \mid^2) = \frac{\mid V \mid^2}{8R_A}(1 - \mid \Gamma_{load} \mid^2) \tag{32}$$

where Γ_{load} represents the losses caused by conjugate mismatching:

$$\mid \Gamma_{load} \mid = \frac{Z_L - Z_A^*}{Z_L + Z_A} \tag{33}$$

based on the Euqations (33) - (32) we can conclude with a result, that losses caused by conjugate mismatch are primarily dependent on input resistance of an antenna $R_A \; = \; R_{rad}+R_{ohm}$. For power delivered to the receiving load is valid:

$$R_{ohm} \uparrow \Rightarrow \; \mid \Gamma_{load} \mid = 0 \tag{34}$$

In limit values approaches to zero values for R_{ohm} will be Γ_{load}, but power delivered to the receiving load will be converge to 0. In biological system we trying to find the equivalent expressing the ohmic losses of an antenna. In this calculation it is important for us to find the biological analogy for R_{rad} and R_{ohm}. This will be part of a future work.

4.2 Microtubule as resonant system

This calculation is based on the MT dipole approximation, which was described earlier in Subchapter 2.2. Because the biological systems that we considering are much smaller than the wavelength of microwave radiation, which is by definition greater than 1 mm, any absorption of energy by the system must take place through the interaction of the field with the dipole moment charge distribution of the system. Proceed by Adair [1] the absorption of energy by a resonant system from a electromagnetic plane wave through a dipole interaction can be expressed in terms of an absorption cross-section, (σ_a) [8] as:

$$\sigma_a(\nu) = 3\frac{\lambda^2}{\pi}\frac{\Gamma_s\Gamma_a}{(\nu-\nu_r)^2+\Gamma^2/4} \tag{35}$$

where Γ_a is absorption width, Γ_s emission width of the system, Γ is the total width ($\Gamma = \Gamma_a + \Gamma_s$), ν_r is resonant frequency, and $\lambda = c/\nu$ is the wavelength of the radiation. The cross-section σ_a is defined as the power absorption per unit incident power flux and has the dimensions of area. If the incident power flux is I [W/m^2], the power (Pa) absorbed by the system is:

$$P_a = I\sigma_a \tag{36}$$

That leads to an increase in energy, (Δw) in the system:

$$\Delta\, w \;=\; P_a \times \tau \;=\; \frac{I\times\sigma_a}{\Gamma_a} \text{ pre } \Gamma_a \;>>\; \Gamma_s \tag{37}$$

The condition, $\Gamma_a >> \Gamma_s$ will generally obtain for biological systems of interest. My goal was to calculate power absorbed by the system, with condition when the frequency of the incident radiation is equal to resonant frequency. I reflected following conditions $(\nu = \nu_r)$, $(\Gamma_a >> \Gamma_s)$. This conditions leads to modification of Equation (35):

$$\sigma_a(\nu) = 3\frac{\lambda^2}{\pi}\frac{\Gamma_s\Gamma_a}{\Gamma^2/4} \;=\; 12\frac{\lambda^2}{\pi}\frac{\Gamma_s\Gamma_a}{\Gamma_a^2+2\Gamma_a\Gamma_s+\Gamma_s^2} = 12\frac{\lambda^2}{\pi}\frac{\Gamma_s}{\Gamma_a+2\Gamma_s+\Gamma_s^2/\Gamma_a} = 12\frac{\lambda^2}{\pi}\frac{\Gamma_s}{\Gamma_a} \tag{38}$$

We need to calculate Γ_a and Γ_s from Equation (38) for absorption cross-section. This calculations are in sections 4.2.1 - 4.2.2.

4.2.1 Emission width Γ_s

Calculation of emission width Γ_s is based on electrodynamics equations. The power P radiated by an oscillating electric dipole [30]:

$$P = \frac{dw}{dt} = \frac{1}{4\pi\varepsilon_0}\frac{d_0^2\omega_0^4}{3c^3} \tag{39}$$

where $\omega_0 = 2\pi c/\lambda$ is radial frequency of the oscillator and $d_0 = q.a$ is the maximal oscillating dipole moment, which are described in terms of an amplitude a and charge q. Then using the energy of the oscillator as:

$$w_o = \frac{1}{2}m\omega^2a^2 \tag{40}$$

where m is the mass of the system. For emission width Γ_s is then valid:

$$\Gamma_s = \frac{P}{w_o} = \frac{1}{4\pi\varepsilon_0}\frac{d_0^2\omega^4}{3v^3}\frac{2}{m\omega^2 a^2} = \frac{2d_0^2\omega^2}{\pi\varepsilon_0 12c^3 m a^2} = \frac{1}{6}\frac{q^2\omega^2}{\pi\varepsilon_0 m c^3} \tag{41}$$

4.2.2 Absorption width Γ_a

The absorption width is related to the relaxation time of the system by basic equation (τ=$1/\Gamma_a$). In the first chapter we used basic lifetime calculations based on an oscillating dipole in homogenous environment. Then basic knowledge of oscillating dipole lifetime gave us a good estimate of relaxation times (absorption width). Then we used several advanced methods for absorption width calculation. First we used calculation performed by Adair [1] which is based on resonant system approximation. Then I calculated absorption width by approaches used in works of Foster [18] and Pokorný [38] which are based on determining the viscous forces and rate of energy losses in a cylinder undergoing longitudinal oscillations in water.

4.2.2.1 Absorption width based on oscillating dipole

In the first step we considered an undriven harmonically oscillating dipole. As the dipole oscillates it radiates energy according to Eq. (39). As a consequence, the dipole dissipates its energy into radiation and its dipole moment decreases. We are interested in calculating the time τ after which the dipole's energy decreases to $1/e$ of its initial value. The natural frequency of the oscillator is ω and its damping constant is γ_0. Because of losses introduced through γ_0 the dipole forms a non-conservative system. The damping rate not only attenuates the dipole strength put also produces a shift in resonance frequency. We simply find:

$$\tau = \frac{1}{\gamma_0} \tag{42}$$

The average energy of a harmonic oscillator is the sum of the average kinetic and potential energy. At time t this average energy reads as:

$$W(t) = \frac{m}{2q^2}[\omega^2 p^2(t) + p^2(t)] = \frac{m\omega^2}{2q^2}|\vec{p_0}|^2 \exp^{-\gamma_0 t} \tag{43}$$

By using the analogy from atomic and molecule physics the energy conservation requires that the decrease in oscillator energy must equal to energy losses, i.e:

$$W(t=0) - W(t) = q_i \int_0^t P(t')dt' \tag{44}$$

where we used *intrinsic quantum yield* q_i. The quantum yield gives the efficiency of the emission process. It is defined as the ratio of the number of photons emitted ($photons_{em}$) to the number of photons absorbed ($photons_{abs}$):

$$q_i = \frac{photons_{em}}{photons_{abs}} \tag{45}$$

The quantum yield Q can also be described by the relative rates of the radiative k_r and non-radiative k_{nr} relaxation pathways, which deactivate the excited state.

$$q_i = \frac{k_r}{k_r + \sum k_{nr}} \tag{46}$$

The maximum emission quantum yield is 1.0 (100 %); each photon absorbed results in a photon emitted. Compounds with quantum yields of 0.10 are still considered quite fluorescent. By using condition for biological systems where $\Gamma_a >> \Gamma_s$ we are expecting quantum yield values to be in ranges close to the zero (for calculation we used value $q_i = 10^{-9}$). It is now straightforward to solve for the decay rate. We appointed Eq. (39) and Eq. (43) into the last equation and obtained:

$$\gamma_0 = q_i \frac{n^3}{4\pi\varepsilon_0\varepsilon} \frac{2q\omega^2}{3mc^3}\ classical \tag{47}$$

This is the classical formula for the atomic decay rate and through Eq. (42) also for the atomic lifetime. It depends on the oscillation frequency and the oscillating particle's mass and charge. We see that the higher the index of refraction of the surrounding medium is, the shorter the lifetimes of the oscillator will be.

4.2.2.2 Absorption width by Adair

My process in absorption width calculation (Γ_a) was following. I considered MT as the cylindrical object of radius (r), length (L), oscillating longitudinally with a frequency $\nu_r = \omega/2\pi$, and amplitude (a), then the retarding force can be expressed approximately as [1]:

$$F_d = \frac{2\eta\pi L\omega a^2}{\ln(v_a/\omega r)} \text{ in condition } r < \frac{v_a}{\omega} < L \tag{48}$$

where v_a is velocity of the acoustic wave in microtubule, η_d dynamic viscosity of the environment. Next I used the energy of oscillator described in Equation (40). Energy lost by friction is given as [1] $dw/dt = F_d\omega a$. Mass of the cylinder (m) is $m = \pi r^2 L\rho$ and for the absorption width (Γ_a) we obtain the equation:

$$\tau = \frac{1}{\Gamma_a} = \frac{w}{dw/dt} = \frac{w}{F_d\omega a} = \frac{1/2m\omega^2a^2}{2\pi\eta_d\omega^2La^2/\ln(v_a/\omega r)} = \frac{m\omega^2a^2\ln(v_a/\omega r)}{4\pi\eta L\omega^2a^2} = \frac{\rho r^2\ln(v_a/\omega r)}{4\eta_d} \tag{49}$$

where ρ is density of the protein, which is the basic mass unit of the MT.

4.2.2.3 Absorption width by Foster

Foster used another way how to calculate absorption width (Γ_a). First step was determining a viscous force on a uniform cylinder of radius R immersed in a fluid, which is undergoing forced sinusoidal oscillation at angular frequency ω in a longitudinal mode. The cylinder is immersed in a fluid of density ρ_{env} and kinematic viscosity η_k. The cylinder is acted on by a shear stress (axial force per unit surface area) F_v:

$$F_v = \eta_d \left.\frac{\partial u}{\partial r}\right|_{r=R} \tag{50}$$

where η_d is the dynamic viscosity of the environment. The momentum equation in cylindrical coordinates can be written [18]:

$$\eta_k \left(\frac{\partial^2 u}{\partial r^2} + \frac{1}{r} \frac{\partial u}{\partial r} \right) = \frac{\partial u}{\partial t} \tag{51}$$

where u is the axial component of the velocity. Foster assumed **non-slip** (stick) boundary condition at the cylinder's surface where $r = R$:

$$u(R, t) = u_0 \cos(\omega t) \tag{52}$$

That is the main difference between the approach which was used by Pokorný [38]. Pokorný assumed **slip** boundary condition. The reason was the phenomena of organized water which reducing the damping of longitudinal vibration compared to free water, due to the existence of sliding surface along the microtubule structure created by this water as was described in Subsection 2.3. The second condition is that the velocity converges to zero far from the cylinder:

$$u(\infty, t) = 0 \tag{53}$$

This boundary value problem is analogous to that of heat diffusion in a solid around a cylinder with an oscillating temperature [18]. Its solution has the form:

$$u(r, t) = u_0 \cos(\omega t) g(r) \tag{54}$$

Substituting Equation (54) into Equation (51) yields:

$$\frac{d^2 g}{dr^2} + \frac{1}{r} \frac{dg}{dr} + \frac{i\omega}{\eta_k} g = 0 \tag{55}$$

whose solutions are modified Bessel's function (first $\mathrm{I}_0(x)$ and the second kind $\mathrm{K}_0(x)$) of the zeroth order.

$$K_0 \left(r \sqrt{\frac{i\omega}{\eta_k}} \right), \; I_0 \left(r \sqrt{\frac{i\omega}{\eta_k}} \right) \tag{56}$$

We reject the I_0 solution which diverges at infinite r and the velocity profile $u(r, t)$ is given as [18]:

$$u(r, t) = \Re \left\{ u_0 \cos(\omega t) \frac{K_0 \left(r \sqrt{\frac{i\omega}{\eta_k}} \right)}{K_0 \left(R \sqrt{\frac{i\omega}{\eta_k}} \right)} \right\} \tag{57}$$

Inserting into Equation (50) and evaluating gives:

$$F_v = -u_0 \cos(\omega t) \eta_d \sqrt{\left(\frac{i\omega}{\eta_k} \right)} \frac{K_1 \left(R \sqrt{\frac{i\omega}{\eta_k}} \right)}{K_0 \left(R \sqrt{\frac{i\omega}{\eta_k}} \right)} \tag{58}$$

The rate of energy loss per unit length of the cylinder, due to viscous drag, is simply:

$$\frac{dE(t)}{dt} = -2\pi R F_v u(t) \tag{59}$$

This is proportional to the kinetic energy $E(t)$ per unit length:

$$E(t) = \frac{1}{2}\pi R^2 \rho u^2(t) \tag{60}$$

This implies that energy is lost to dissipative forces as a single exponential process with relaxation time constant τ:

$$\tau = \frac{1}{\Gamma_a} = \frac{-E}{dE/dt} = \frac{1}{4}\frac{\rho R u(t)}{F_v} \tag{61}$$

for $u(t)$ was used expression in Equation (52). Then I substitute relaxation time into previous Equation (38).

4.2.2.4 Absorption width by Pokorný

Calculation made by Pokorný in his work [38] is based on the same basis as Foster calculation (Subsection 4.2.2.3) except for one main difference. Pokorný assumed **slip** boundary condition. The reason is the phenomena of organized water which reduces the damping of longitudinal vibrations compared to free water, due to the existence of sliding surface along the microtubule structure created by this water (Subsection 2.3). He assumed longitudinal harmonic vibrations along the axis of the MT. For the sake of implicity he neglected dependence of the velocity u on the distance z around the microtubular axis. Also the properties of the assumed cylindrical model do not depend on the angle of revolution along the MT axis. Then he also used the Equation (50). Thus the momentum equation:

$$r^2\frac{\partial^2 u}{\partial r^2} + r\frac{\partial u}{\partial r} - i\frac{\omega}{u}r^2 = 0 \tag{62}$$

Solution can be also as in the case of Foster found by using Kelvin's function in the form [38] (condition (53)). The solution of the Equation (62) can be than written as (57). The viscous force act on the outer surface of the slip layer causing damping of its vibrations. The viscous force F_v per unit length from Equations (50) and (57):

$$F_v = -u_0 \exp\left[i(\omega t + \frac{\pi}{4})\right]\sqrt{\omega\rho_{env}\eta_d}\frac{K_1\left(R\sqrt{\frac{i\omega}{\eta_k}}\right)}{K_0\left(R\sqrt{\frac{i\omega}{\eta_k}}\right)}Si = -\beta u_0 \exp\left(i\omega t\right) \tag{63}$$

where β - the force for unit amplitude - is given by:

$$\beta = \exp\left(i\frac{pi}{4}\right)\sqrt{\omega\rho_{env}\eta_d}\frac{K_1\left(R\sqrt{\frac{i\omega}{\eta_k}}\right)}{K_0\left(R\sqrt{\frac{i\omega}{\eta_k}}\right)}Si \tag{64}$$

and $Si = 2\pi R$ is the area of the cylindrical surface of unit length. The total vibration energy stored in the microtubule per unit length may be determined from the kinetic energy in the form:

$$E = \frac{1}{4}\pi(R_m^2 - R_{m0}^2)\rho U_0^2 \tag{65}$$

where R_m and R_{m0} are the outer and the inner radius of the MT. For the average rate of energy loss per unit length caused by viscous damping we get [38]:

$$E' = -\frac{1}{2}|\beta|U_0^2 \tag{66}$$

Using Equations (65) and (66) the relaxation time τ may be evaluated from the relation (similar to Foster [18] Subsection 4.2.2.3):

$$\tau = \frac{1}{\Gamma_a} = \frac{E}{|E'|} = \frac{1}{2}\pi(R_m^2 - R_{m0}^2)\rho_{env}|\beta|\frac{\omega^2}{f^2} \tag{67}$$

where f is the elastic force constant per unit length (slip condition induction) which can be determined from the dynamic shear modulus G in the form:

$$f = \frac{GSi}{\Delta R} \tag{68}$$

Then I substitute relaxation time into previous Equation (38).

4.3 Water absorption

Based on the comparison of water absorbtion with given volume containing a number of microtubules we can deduce the final results of microwave absorption of microtubules which are dissolved in a solution. My goal was to calculate the power absorbed in water in the case of harmonic electromagnetic wave passing through lossy environment. When the electromagnetic wave plane goes through lossy environment the non-zero electric field intensity will induce electric current in the same direction as the electric field intensity (Fig. 18).

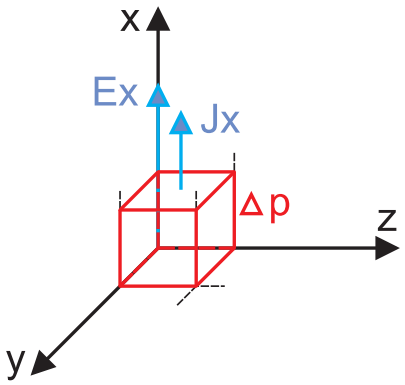

Fig. 18: Loss per unit volume.

The current density can be determined from Ohm's law as:

$$J = \sigma_{ef}E \tag{69}$$

where σ_{ef} is total effective conductivity of the environment. According to Joule law the power which is converted into heat is given as:

$$\Delta p_\vartheta = JE = \sigma_{ef}E^2 \tag{70}$$

In the case of a plane wave, all variables are expressed by the amplitude:

$$\Delta p_\vartheta = \sigma_{ef} E^2 = \frac{1}{2}\sigma_{ef} E^2 \tag{71}$$

The amplitude parameter is most reduced in the direction of **z** axis by:

$$e^{-\alpha z} \tag{72}$$

Thus, in the general point is valid with respect to the square of the electric field:

$$\Delta p_\vartheta(z) = \frac{1}{2}\sigma_{ef} E^2 e^{-2\alpha z} \tag{73}$$

where α is attenuation factor of the environment. We reach the power dissipation by integrating the bulk density of losses by the Equation (73), so we obtain total losses in block:

$$\Delta P_\vartheta = \iiint\limits_V \Delta p_\vartheta \, dV = \int_{z1}^{z2}\int_{y1}^{y2}\int_{z1}^{z2} \Delta p_\vartheta \, dx\, dy\, dz = \int_{z1}^{z2}\int_{y1}^{y2}\int_{z1}^{z2} \frac{1}{2}\sigma_{ef} E^2 e^{-2\alpha z} \, dx\, dy\, dz \tag{74}$$

Sections of the integration can be determined from the volume of the cube V, $(a = x, y, z)$. And substitute to:

$$\Delta P_\vartheta = \iiint\limits_V \Delta p_\vartheta \, dV = \frac{1}{4}\frac{\sigma_{ef} E^2}{\alpha}\left[1 - e^{-2\alpha z1}\right](x1 - x0)(y1 - y0) \tag{75}$$

From macroscopic point of view is not possible for us to practically distinguish individual contributions to losses at constant frequency. Therefore, in practical expression im using the effective conductivity which includes all conductivity losses:

$$\sigma_{ef} \; = \; \mathrm{tg}(\delta)\omega\varepsilon_0\varepsilon_r \tag{76}$$

Calculation of the attenuation factor of the environment (α) by using Equation [23]:

$$\alpha = \omega\sqrt{\left[\frac{\varepsilon\mu}{2}\left(-1 + \sqrt{1 + \frac{\sigma_{ef}^2}{\omega^2\varepsilon^2}}\right)\right]} \tag{77}$$

and absolute permeability of water $\mu = \mu_0\mu_r$ (μ_0 is permeability of free space and μ_r permeability of water) together with total effective conductivity of saline (σ_{ef}) calculated by Equation (76).

For the electric field $(\vec{E})$ calculation of the transversal electromagnetic wave TEM was used approach described in [4], [35]. First we use Poynting vector as the representation of the directional energy flux density of an electromagnetic field:

$$\vec{S} = \vec{E}\,\mathrm{x}\,\vec{H} \tag{78}$$

For time-periodic sinusoidal electromagnetic fields, the average power flow per unit time is often more useful, and can be found by treating the electric and magnetic fields as complex vectors. Real density of ceding power is real part of mean value Poynting vector:

$$\vec{S} = \frac{1}{2}\vec{E}\,\mathrm{x}\,\vec{H}^{*} \tag{79}$$

$$\vec{S} = Re\,\vec{S} \tag{80}$$

Intensity of the EM wave can be now related to the amplitude of the Poynting real power vector as:

$$I = Re|\vec{S}| = \frac{1}{2}Y|\vec{E}|^{2} \tag{81}$$

where Y is characteristic admittance:

$$Y = \sqrt{\frac{\varepsilon_0}{\mu_0}} \tag{82}$$

5 Absorption model for single microtubule

This section contains results of resonant absorption model for single microtubule. We used the approach based on resonant system approximation which was described in the Subchapter 4.2. Absorption width was calculated on the basis of dipole approximation and followed by approximations which used Adair, Foster and Pokorný (see Subchapters 4.2.2.2, 4.2.2.3, 4.2.2.4). Calculations were performed for an incident TEM wave interacting with one microtubule in an aqueous solution. The frequency of the incident TEM wave corresponds to the frequency of the first longitudinal MT stretching mode. First we made absorption calculation for three different MT lengths (2, 10, 20 μm). Then we calculated absorption for an angular dipole moment distribution 5.1, various dipole moments of tubulin heterodimer 5.2 and on the end we combined these two calculations together in Subchapter 5.3.

First calculation was for 2 μm microtubule oriented parallel to the electric field. The frequency of the incident TEM wave is equal to the frequency of the first longitudinal stretching mode (2 μm MT) ($\nu_r = 2.57$ GHz).

Microtubule charge was obtained from the dipole moment value of tubulin heterodimer. I used a value $p_x = 337$ D calculated in the work of Tuszynski et al. [45]. For distance d between monomers we used value d = 8 nm [33]. Charge of one tubulin heterodimer was calculated from the Equation (1). Subsequently we deduced the number of heterodimers in 2 μm MT consisted of thirteen protofilaments to $N_{dimer} = 3250$. Then we performed the calculation of microtubule charge $q = 4.6.10^{-16}$ C. *The angular frequency* was calculated for the resonant frequency equaled to the microtubule array oscillating at the first longitudinal stretching mode by using the formula $\omega = 2\pi\nu_r$ to $\omega = 1.6.10^{10}$ Rad.s^{-1}. Then we performed the *microtubule weight* calculation based on the knowledge of dimer subunit weight $m_{alpha} = 55$ kD [45] to $m = 5.93.10^{-19}$ Kg.The *speed of electromagnetic wave* in the environment was calculated from the environment permittivity. Since the environment in which MT is located (I used 0.9% Saline) is lossy, we can describe it in the form of complex permittivity (18). Then we used this knowledge to refractive index calculation:

$$n = \sqrt{\varepsilon_r \mu_r} = 8.4 \tag{83}$$

where $\varepsilon_r = 72$ [24] (the value corresponds to the real part of environment permittivity 0,9% Saline for resonance frequency). Speed of the electromagnetic wave in a saline solution was determined by the equation:

$$v = \frac{c}{n} = 4.46.10^7\, m/s. \tag{84}$$

we took these values and used Euqation (41) for emission width calculation $\Gamma_s = 1.24.10^{-5}$ Hz. As the value of *MT density* we used standard protein value $\rho = 1.35$ g.cm^{-3} from work [17]. For microtubule *radius* the value $r = 12.5$ nm was used [27] and for *water dynamic viscosity* $\eta_d = 1.002.10^{-3}$ Pa.s (at room temperature of 20° C). For speed of acoustic wave in microtubule we used knowledge of MT length, $L = 2\,\mu$m, and formula $v_a = 2L\nu_r$ with result for final speed as $v_a = 10285$ m.s^{-1}. Then we substituted these values into the Equation (49) and calculated the absorption width Γ_a=4.83.10^9 Hz.
Then we performed absorption width calculation for Foster (4.2.2.3) and Pokorný (4.2.2.4)

approximation. In Foster's relaxation time calculation (61) standard protein density value and MT radius was used. We substituted same values into initial speed $u_0 = v_a$, and simplified function ($\cos(\omega t)$) by using effective value given as $a/\sqrt{2}$. For *kinematic viscosity* the value $\eta_k = 1.002.10^{-6}\,\mathrm{m}^2.\mathrm{s}^{-1}$ was used. For outer and inner diameter of MT we used values $R_m = 8.5.10^{-9}$, $R_{m0} = 12.5.10^{-9}\,\mathrm{m}$ in relaxation time calculation (67). Calculations were performed for thickness of the slip layer ($\Delta R = 0.25\,\mathrm{nm}$) with dynamic shear modulus $G = 5\,\mathrm{N.m}^{-2}$.
We proceeded in the same way for other MT lengths. Change of following parameters was considered: Change in the total charge q, the change in angular frequency ω by the change in resonant frequency ν_r, the change in mass m, which it relates to changes in the wave lengths of the incident radiation λ. For clarity, I present the calculations results of absorption for the four lengths (2, 10, 20 μm) of microtubules in Tables 2 - 5.

L [μm]	ν_r [GHz]	λ [mm]	Γ_s [Hz]	τ [s]	Γ_a [Hz]	σ_{abs} [cm^2]	P_a [dB]
2	2.57	13.7	$1.2.10^{-5}$	$3.8.10^{-14}$	$2.6.10^{13}$	$3.4.10^{-22}$	-214
10	1.42	24.3	$1.9.10^{-5}$	$1.2.10^{-13}$	$8.5.10^{12}$	$5.3.10^{-21}$	-202
20	1.28	26.9	$3.3.10^{-5}$	$1.4.10^{-13}$	7.10^{12}	$1.2.10^{-20}$	-199

Tab. 2: Electromagnetic absorption by single microtubule (P_a). Relaxation time (τ) approach based on dipole approximation 4.2.2.1. (L - MT length, λ - incident wavelength, ν_r - resonant freq., Γ_a, Γ_s - absorption and emission width, σ_{abs} - absorption cross-section).

L [μm]	ν_r [GHz]	λ [mm]	Γ_s [Hz]	τ [s]	Γ_a [Hz]	σ_{abs} [cm^2]	P_a [dB]
2	2.57	13.7	$1.2.10^{-5}$	$0.21.10^{-9}$	$4.8.10^{9}$	$1.8.10^{-18}$	-177
10	1.42	24.3	$1.9.10^{-5}$	$0.29.10^{-9}$	$3.4.10^{9}$	$1.3.10^{-17}$	-168
20	1.28	26.9	$3.3.10^{-5}$	$0.33.10^{-9}$	$3.0.10^{9}$	$2.9.10^{-17}$	-165

Tab. 3: Electromagnetic absorption by single microtubule (P_a). Relaxation time (τ) approach used by Adair 4.2.2.2. (L - MT length, λ - incident wavelength, ν_r - resonant freq., Γ_a, Γ_s - absorption and emission width, σ_{abs} - absorption cross-section).

L [μm]	ν_r [GHz]	λ [mm]	Γ_s [Hz]	τ [s]	Γ_a [Hz]	σ_{abs} [cm^2]	P$_a$ [dB]
2	2.57	13.7	$1.2.10^{-5}$	$0.26.10^{-10}$	37.10^9	$2.4.10^{-19}$	-186
10	1.42	24.3	$1.9.10^{-5}$	$0.34.10^{-10}$	29.10^9	$1.5.10^{-18}$	-178
20	1.28	26.9	$3.3.10^{-5}$	$0.35.10^{-10}$	28.10^9	$3.2.10^{-18}$	-174

Tab. 4: Electromagnetic absorption by single microtubule (P$_a$). Relaxation time (τ) approach used by Foster 4.2.2.3. (L - MT length, λ - incident wavelength, ν_r - resonant freq., Γ_a, Γ_s - absorption and emission width, σ_{abs} - absorption cross-section).

L [μm]	ν_r [GHz]	λ [mm]	Γ_s [Hz]	τ [s]	Γ_a Hz	σ_{abs} [cm^2]	P$_a$ [dB]
2	2.57	13.7	$1.2.10^{-5}$	2.7	0.36	$2.5.10^{-8}$	-76
10	1.42	24.3	$1,9.10^{-5}$	0.7	1.5	$3.3.10^{-8}$	-75
20	1.28	26.9	$3.3.10^{-5}$	0.5	1.9	$4.7.10^{-8}$	-73

Tab. 5: Electromagnetic absorption by single microtubule (P$_a$). Relaxation time (τ) approach used by Pokorný 4.2.2.4. (L - MT length, λ - incident wavelength, ν_r - resonant freq., Γ_a, Γ_s - absorption and emission width, σ_{abs} - absorption cross-section).

The results of calculation shows major differences between relaxation time calculations which lead to differences between MT absorption. We can clearly see that power absorbed by MT is dependent on absorption width and is proportional to its length. Largest absorption was calculated for approximation with **slip** condition. This is due to the smallest attenuation of microtubule oscillations.

5.1 Single microtubule absorption for various angles of microtubule orientation

This subchapter describes calculated values of absorbed power (P_a) and relaxation time (τ) by single microtubule for variable angle of microtubule orientation. The absorbed power of resonant system is clearly dependent on the angle of orientation (θ) between the vectors of incident electric field and the dipole moment of tubulin heterodimer in Fig. 19 - 20. This allows us to consider dipole moment dependence on the angle between these two vectors. Based on this angle we can introduce the variable of effective dipole moment (p_{eff}) as:

$$p_{eff} = p\cos^2(\theta) \tag{85}$$

As was written in the Subsection 2.2 the microtubule dipole moment is not primarily oriented radially to the axis but there is a small contribution oriented in the direction of the axis X.

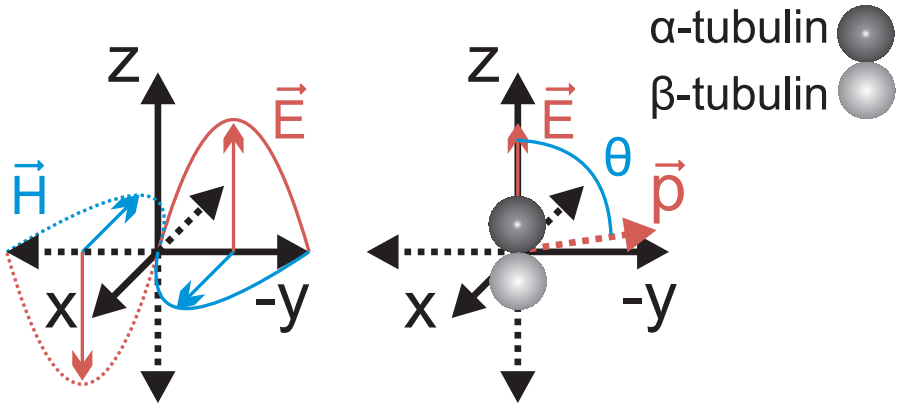

Fig. 19: Angle between the incident wave and tubulin heterodimer dipole moment.

Substituting into the Equation (85) we obtained dipole moment angle dependence shown in Fig. 21 (calculated for total dipole moment of the MT with three different lengths 2, 10, 20μm). Absorption was calculated for all four different relaxation time approaches for three different MT lengths with variable dipole orientation to incident electric field.

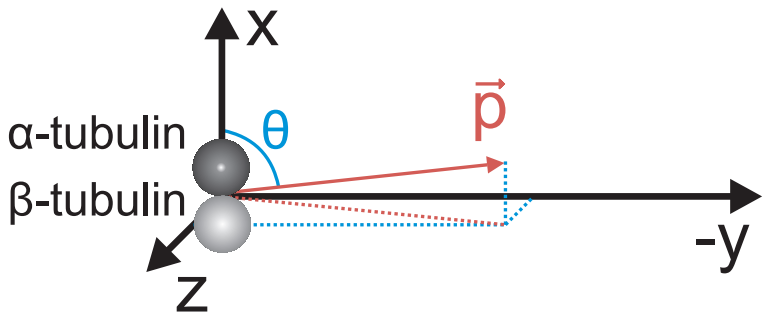

Fig. 20: Orientation of the tubulin dipole moment calculated from the crystallographic data.

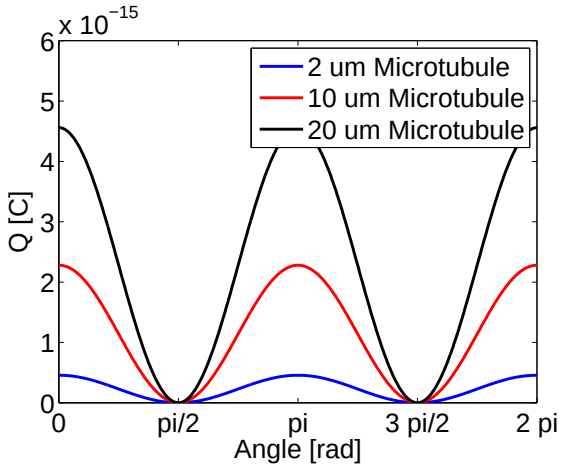

Fig. 21: Effective dipole moment of the MT as a function of angle between the vector of the incident electric field and the MT dipole moment (calculated for p=337 D).

The maximum effective dipole moment occurs when the vector of electric field is parallel to dipole moment vector. The lowest effective dipole moment is when the dipole moment is perpendicular to the vector of electric field.

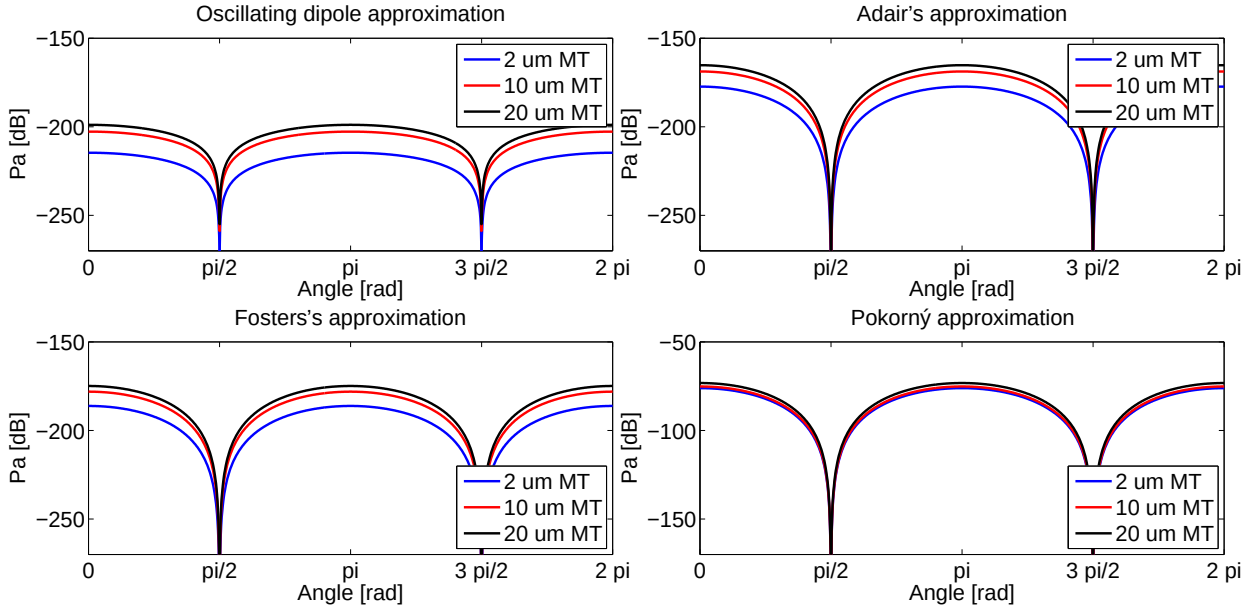

Fig. 22: Angular dependence of the single microtubule absorption (P_a) for three MTs lengths (2, 10, 20 μm) by using all four different relaxation time calculations.

From the angular dependence by the single microtubule absorption (Figure 22) it is clearly visible that absorption is dependent on the position towards the electric field and on the MT length. With increased length the absorption increases. The maximum absorption is again achieved for relaxation time, which were calculated with **slip** condition. The comparison of angular dependence for single MT is shown in Figure 23.

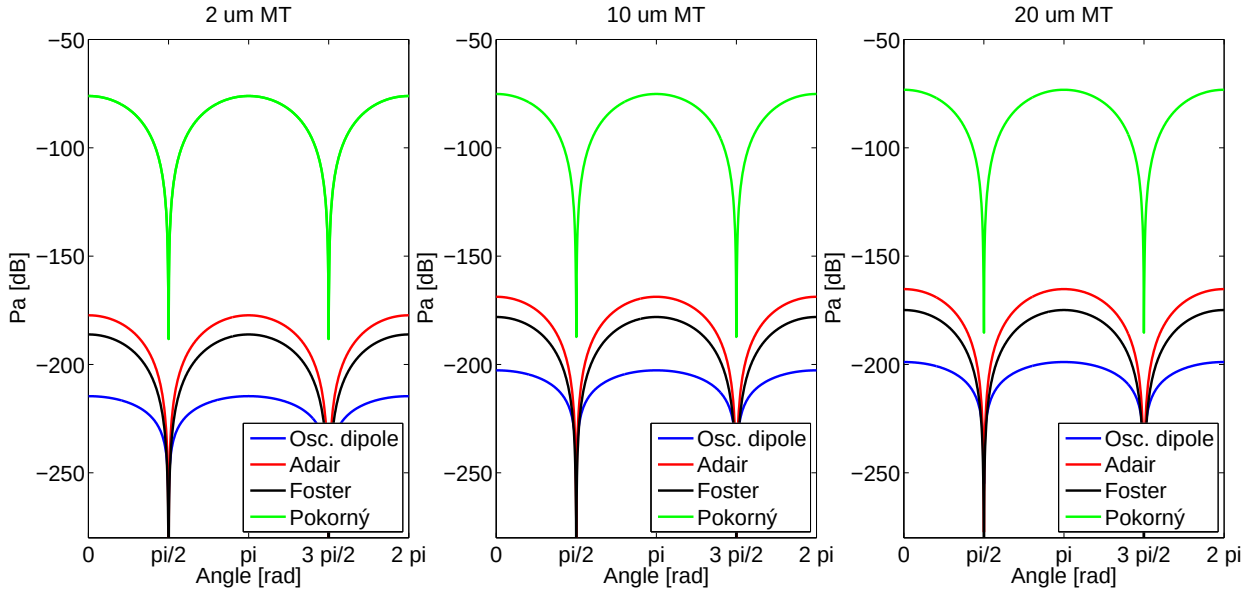

Fig. 23: Angular dependence (comparison) of the single microtubule absorption (P_a) for three MTs lengths (2, 10, 20 μm) by using all four different relaxation time calculations.

5.2 Single microtubule absorption for various magnitudes of dipole moment of tubulin heterodimer

This subchapter describes calculated values of absorbed power (P_a) in microtubules (Figures 24 - 25) for various magnitudes of dipole moment of tubulin heterodimer.

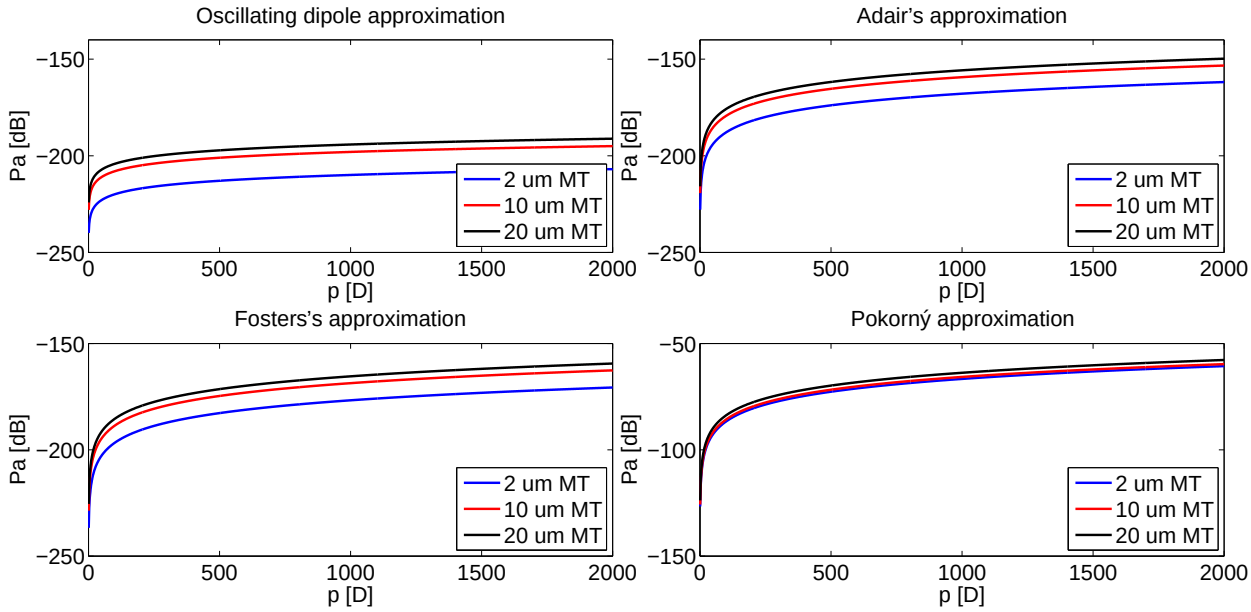

Fig. 24: Single microtubule absorption (P_a) for various magnitudes of dipole moment (p = 0 - 2000 D) of tubulin heterodimer for three MTs lengths (2, 10, 20 μm) by using all four different relaxation time calculations.

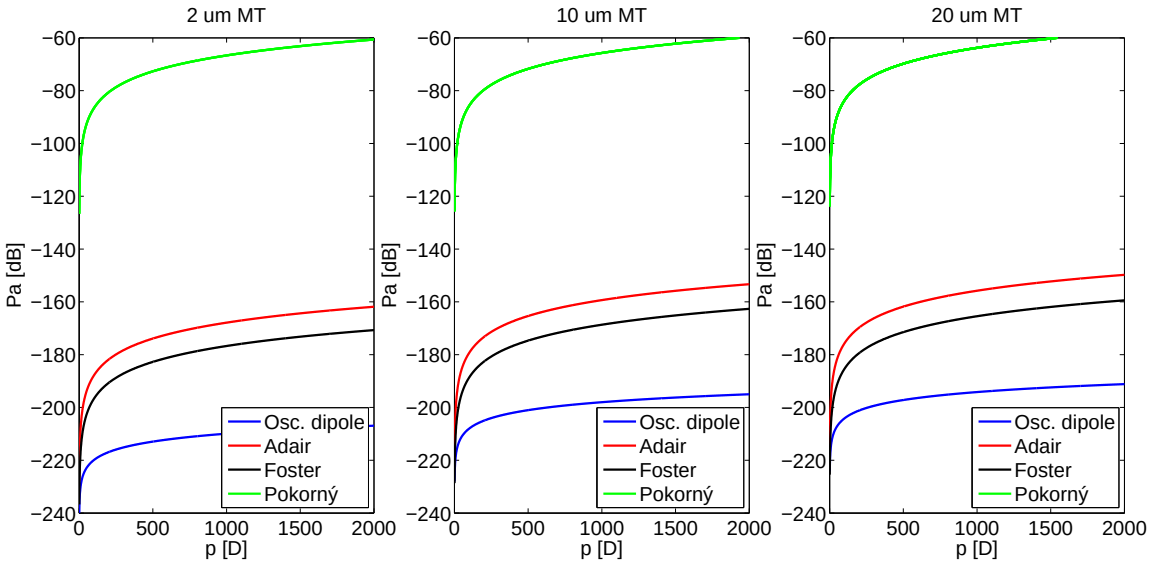

Fig. 25: Comparison of single microtubule absorption (P_a) for various magnitudes of dipole moment (p = 0 - 2000 D) of tubulin heterodimer for three MTs lengths (2, 10, 20 μm) by using all four different relaxation time calculations.

5.3 Single microtubule absorption for various magnitudes of dipole moment and orientation of tubulin heterodimer

We combined results from previous two subchapters in to three-dimensional plots for absorption. Results of calculation are shown in Figures 26 - 28.

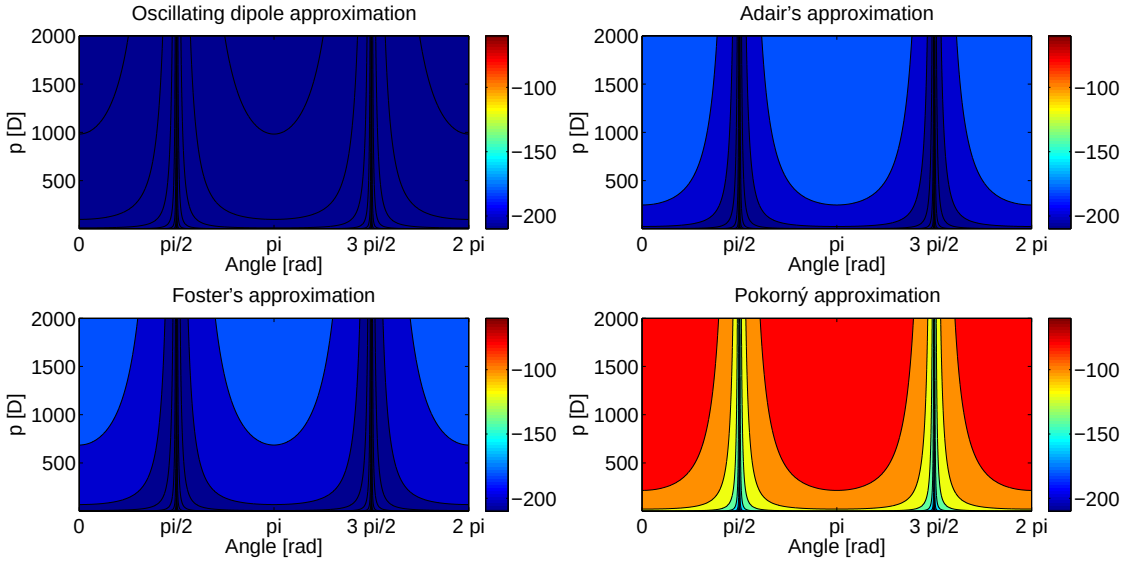

Fig. 26: Single 2μm MT absorption for various magnitudes of dipole moment (p = 0 - 2000 D) of tubulin heterodimer and angle distribution by using all four different relaxation time calculations.

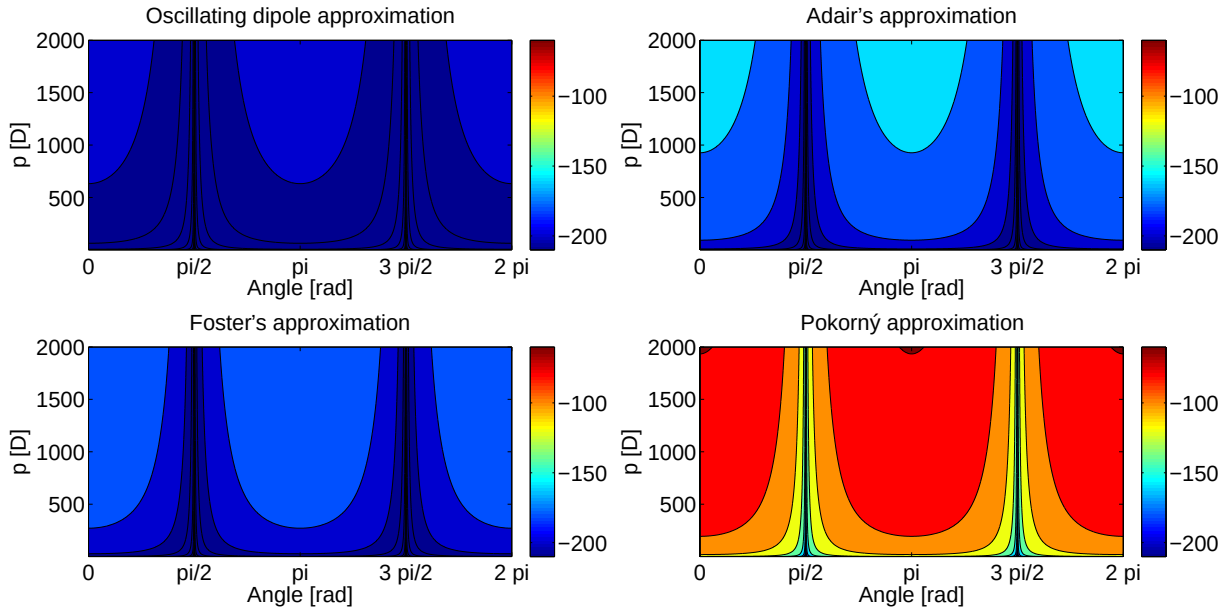

Fig. 27: Single 10μm MT absorption for various magnitudes of dipole moment (p = 0 - 2000 D) of tubulin heterodimer and angle distribution by using all four different relaxation time calculations.

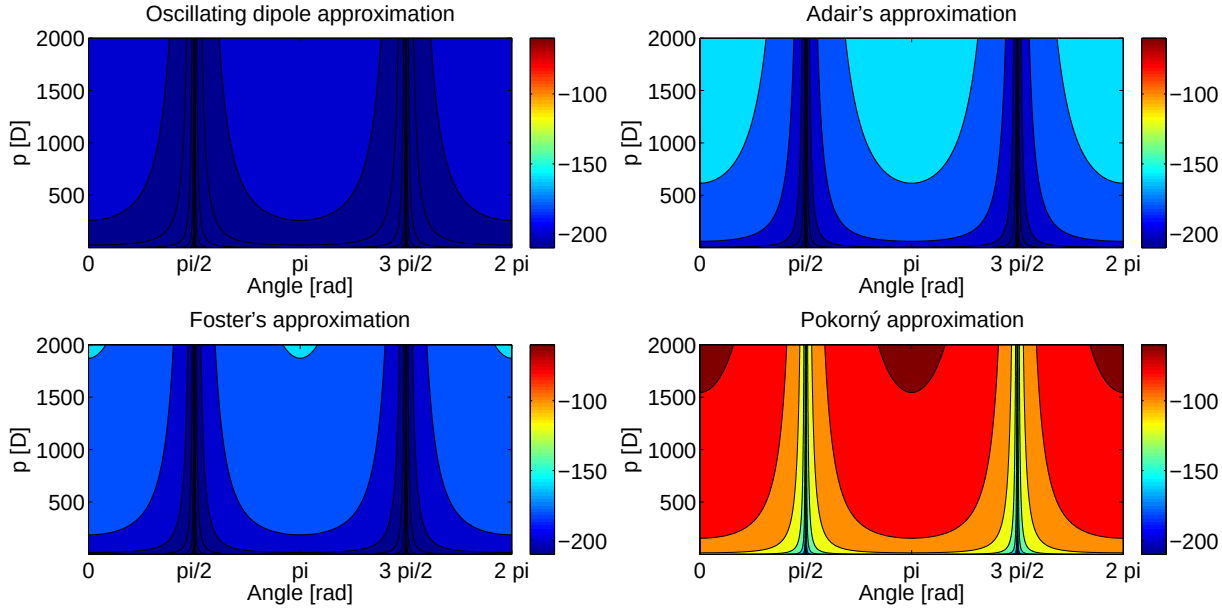

Fig. 28: Single 20μm MT absorption for various magnitudes of dipole moment (p = 0 - 2000 D) of tubulin heterodimer and angle distribution by using all four different relaxation time calculations.

6 Absorption model for microtubules in solution

The following sections deals with the calculation of microtubules absorption in an aqueous environment with MT concentration of 1 mg/ml by using resonant system approach which was described in Subchapter 4.2. Calculations were performed for incident TEM wave and 50 μl of an aqueous solution. Frequency of incident TEM wave corresponds to the frequency of the first longitudinal stretching mod. In absorption model we assumed that all MT are arranged parallel to the axis of the vector $\vec{E}$ and at the same time we neglected the mutual interaction (MTs all have the same cross-sections). First we made absorption calculation for three different lengths (2, 10, 20 μm) (see Subchapter 6.1). In Subchapter 6.2 we calculated absorption for various magnitudes of dipole moment $p = 0$ - 2000 D of tubulin heterodimer. We compared microtubules absorption with water absorption by a given volume. Then in Subchapter 6.3 absorption calculation for different values of environment viscosity $\eta_d = 10^{-6} - 10^{-2}$ Pa was modeled, and these results were combined together in Subchapter 6.4. At the end we calculated MTs absorption with different lengths based on Gaussian distribution 6.5.
For experimental studies it was necessary to calculate water absorption (V=50μl) for resonant frequency and compare it with MTs absorption. Environment attenuation factor of 0.9% saline was calculated by the Equation (77) as $\alpha = 63\,\mathrm{m}^{-1}$. Electric field intensity entering the aqueous E was determined from Equation (81) where the power density $I = 1\,\mathrm{W.m}^{-2}$ enters the water cube. Characteristic admittance of the environment Y was calculated from Equation (82). Final values were substituted into the Equation (75). Power absorbed by water with 50 μl volume was then calculated as $P_\vartheta = 11.6.10^{-3}$ W, P_ϑ = -19 dB. In the same way, we proceeded in determining water absorption for other MT lengths.

6.1 Absorption for variable microtubule lengths

This subchapter describes calculated values of absorbed power (P_a) in microtubules with three different lengths (2, 10, 20 μm) based on Adair and Foster approach (Tables 6 - 7).

L [μm]	ν_r [GHz]	λ [mm]	Γ_s [Hz]	τ [s]	Γ_a [Hz]	σ_{abs} [cm^2]	P$_a$ [dB]	P_ϑ [dB]
2	2.57	13.7	$1.2.10^{-5}$	$0.21.10^{-9}$	$4.8.10^{9}$	$1.6.10^{-7}$	-68	-19.3
10	1.42	24.3	$1.9.10^{-5}$	$0.29.10^{-9}$	$3.4.10^{9}$	$2.2.10^{-7}$	-66	-19.2
20	1.28	26.9	$3.3.10^{-5}$	$0.33.10^{-9}$	$3.0.10^{9}$	$2.5.10^{-7}$	-65	-19.2

Tab. 6: Electromagnetic absorption of MTs in solution (P$_a$). Relaxation time (τ) approach used by Adair 4.2.2.2. (L - MT length, λ - incident wavelength, ν_r - resonant freq., Γ_a, Γ_s - abs. and emission width, σ_{abs} - absorption cross-section, P$_\vartheta$ - water absorption).

My first step was calculating the number of microtubules in solution with concentration of 1 mg/ml in 50 μl. From knowing mass of the number of MTs in solution there number is $N_{MT} = 8.42.10^{10}$ for 2 μm length. Then I deduced the absorption cross-section and power absorbed by microtubules from Equation 36.

L [μm]	ν_r [GHz]	λ [mm]	Γ_s [Hz]	τ [s]	Γ_a [Hz]	σ_{abs} [cm^2]	P$_a$ [dB]	P_ϑ [dB]
2	2.57	13.7	$1.2.10^{-5}$	$0.26.10^{-10}$	37.10^9	$2.0.10^{-8}$	-77	-19.3
10	1.42	24.3	$1.9.10^{-5}$	$0.34.10^{-10}$	29.10^9	$2.6.10^{-8}$	-75	-19.2
20	1.28	26.9	$3.3.10^{-5}$	$0.35.10^{-10}$	28.10^9	$2.7.10^{-8}$	-74	-19.2

Tab. 7: Electromagnetic absorption of MTs in solution (P$_a$). Relaxation time (τ) approach used by Foster 4.2.2.3. (L - MT length, λ - incident wavelength, ν_r - resonant freq., Γ_a, Γ_s - absorption and emission width, σ_{abs} - absorption cross-section, P$_\vartheta$ - water absorption).

6.2 Absorption for various dipole moment of tubulin heterodimer

This subchapter describes calculated values of absorbed power (P_a) in microtubules with three different lengths (2, 10, 20 μm) for various magnitudes of dipole moment of tubulin heterodimer p = 0 - 2000 D. Results of calculation are shown in Figure 29.

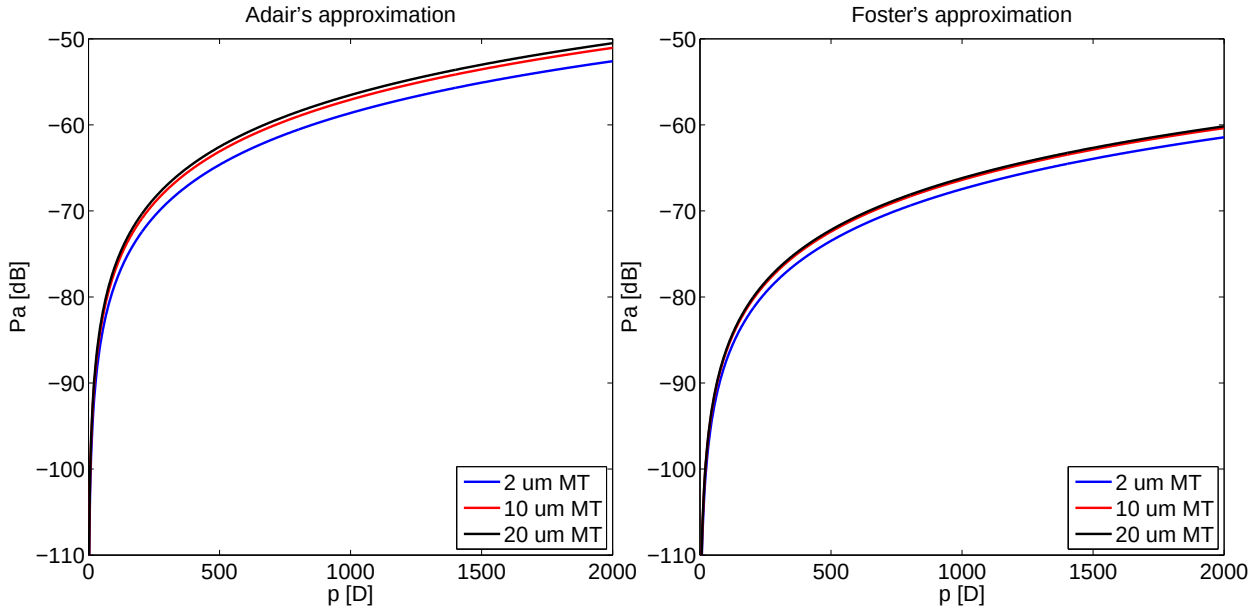

Fig. 29: Electromagnetic absorption of MTs in solution for various dipole moment (p = 0 - 2000 D) of tubulin heterodimer for three MTs lengths (2, 10, 20 μm) with Adair's and Foster's relaxation time calculation.

From Figure 29 we can see that absorption increases with microtubule length. Also we can see the increasing trend of absorption with larger dipole moment. The largest absorption is for 20 μm MTs. The real values of absorption might be smaller because of the variable length of MTs in the environment and also because of the smaller values for dipole moment which was calculated by many authors like Tuszynski et al. [45].

6.3 Absorption for various environment viscosity

This subchapter shows calculated results of absorbed power (P_a) in microtubules with three different lengths (2, 10, 20 μm) for variable values of environment viscosity $\eta_d = 10^{-6}$ - 10^{-2} Pa.s. Results of calculations are shown in Figure 30. The reasons for choosing the variable environment viscosity are well documented in articles [43], [19]. In short we can say that changes in viscosity are exponential in length, which means that they are very sharp near the fundamental length scale. The decreasing size of a floating object may result in viscosity change by 5 - 6 orders of magnitude. That's the main reason of the variable environment viscosity.
We can observe that the environment viscosity is the main factor in MTs absorption. The absorption varies from the lowest value of approximately -85 dB to maximum of -35 dB. This result shows us that the process of absorption is mainly dependent on the environment viscosity in the cell. The maximum of absorption was again corresponding to population with longest microtubules (20 μm), but there are no significant differences between 10 to 20 μm lengths, due to similar resonant frequencies.

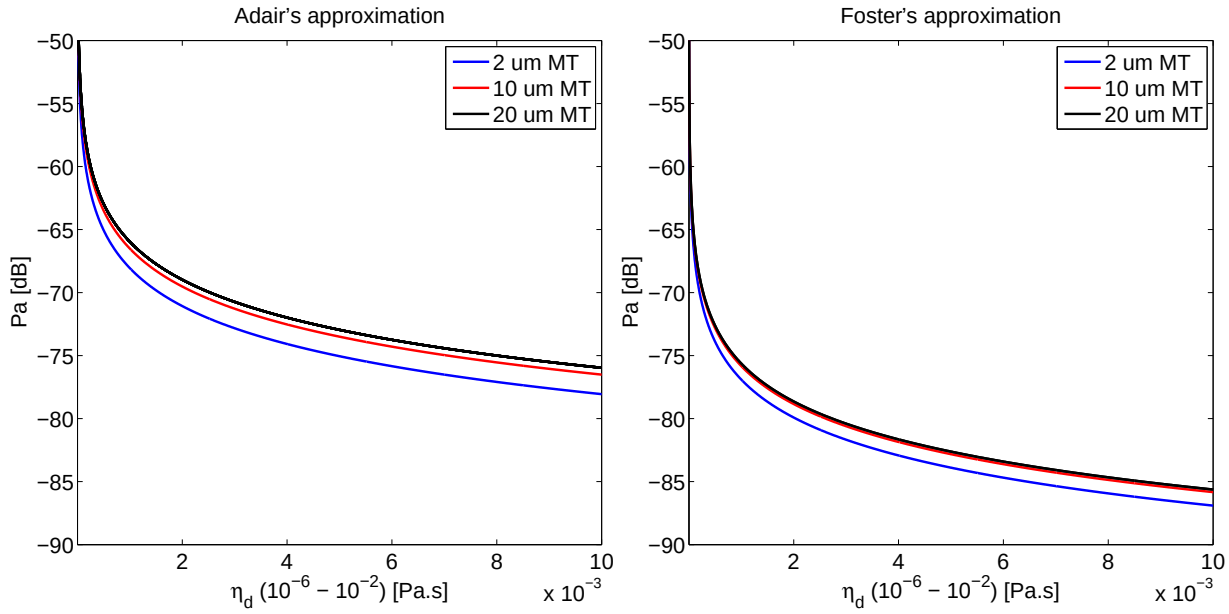

Fig. 30: Electromagnetic absorption of MTs in solution for various environment viscosity ($\eta_d = 10^{-6}$ - 10^{-2} Pa.s) for three MTs lengths (2, 10, 20 μm) with Adair's and Foster's relaxation time calculation.

6.4 Absorption for various dipole moments & viscosity

Subchapter shows calculated results of absorbed power (P_a) in 2, 10, 20 μm microtubules in solution for variable values of environment viscosity $\eta = 10^{-6}$ - 10^{-2} Pa.s and variable values of dipole moment $p = 0$ - 2000 D. Results are illustrated in Figures 31 - 36.

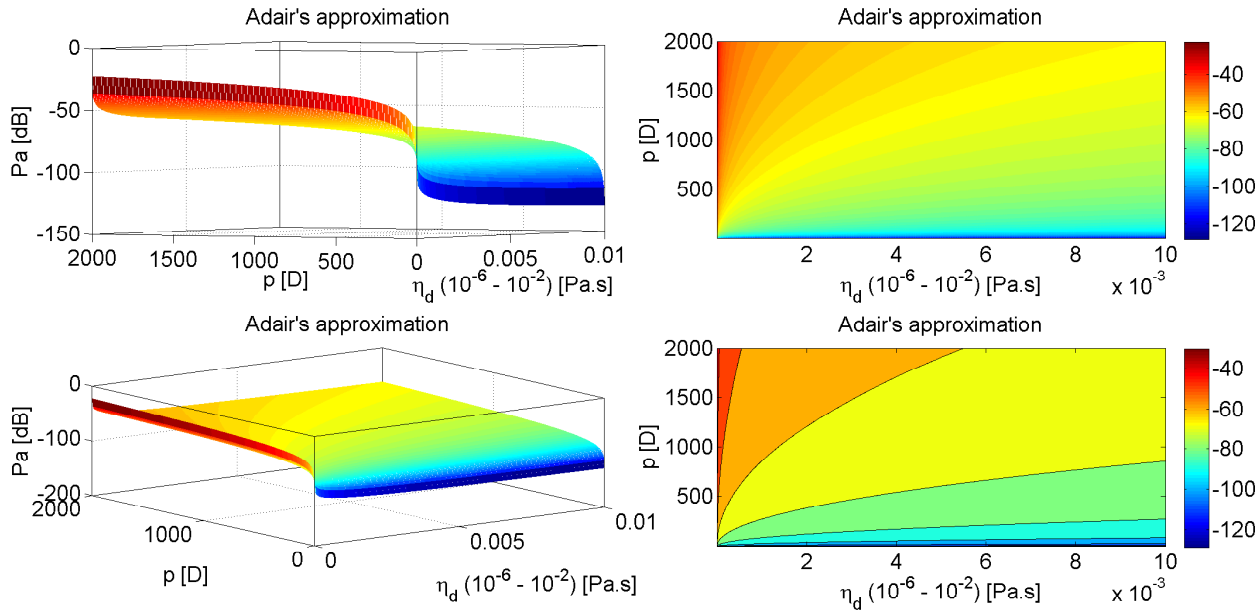

Fig. 31: Adair's absorption of 2 μm MTs in solution for various environment viscosity ($\eta_d = 10^{-6}$ - 10^{-2} Pa.s) and dipole moment (p = 0 - 2000 D) of tubulin heterodimer.

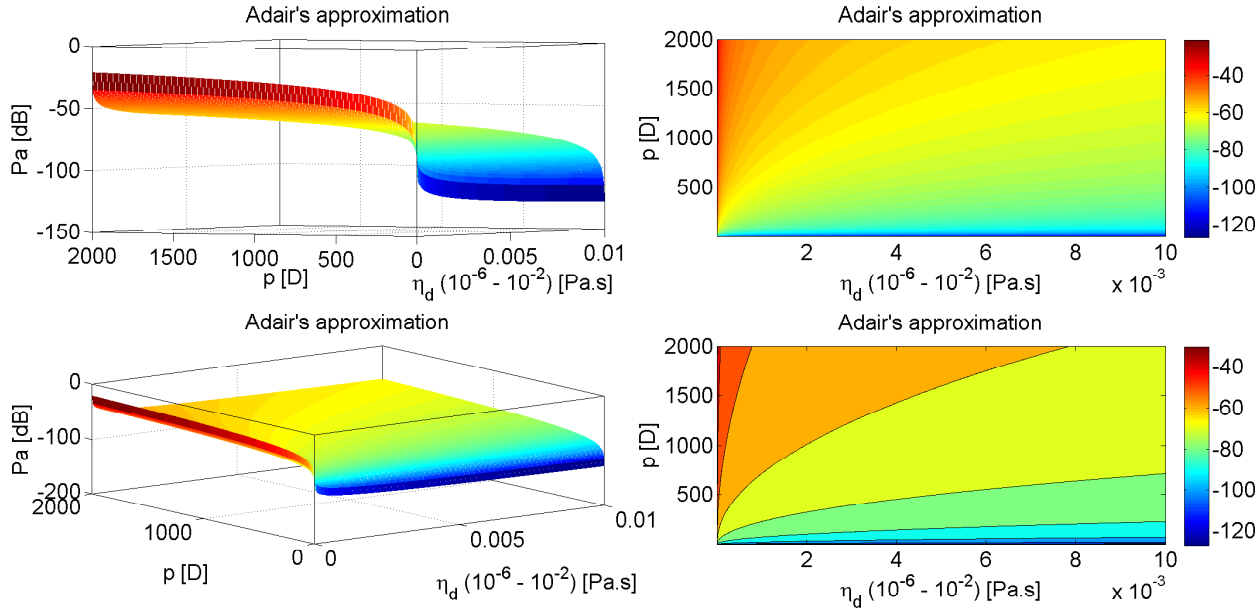

Fig. 32: Adair's absorption of 10 μm MTs in solution for various environment viscosity ($\eta_d = 10^{-6}$ - 10^{-2} Pa.s) and dipole moment (p = 0 - 2000 D) of tubulin heterodimer.

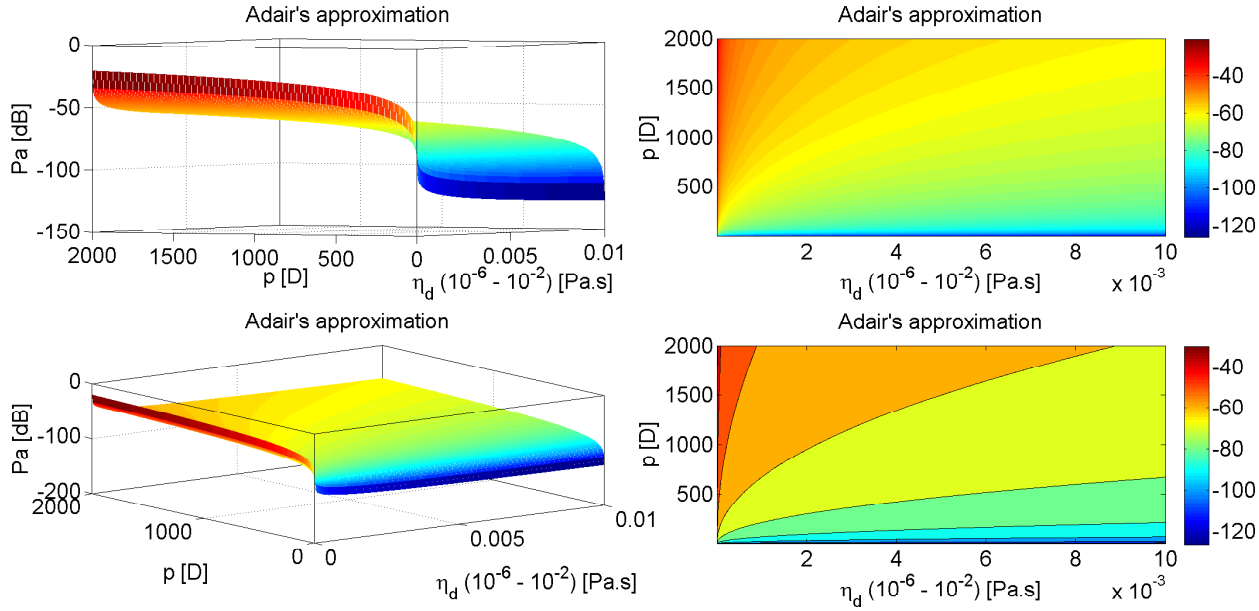

Fig. 33: Adair's absorption of 20 μm MTs in solution for various environment viscosity ($\eta_d = 10^{-6}$ - 10^{-2} Pa.s) and dipole moment (p = 0 - 2000 D) of tubulin heterodimer.

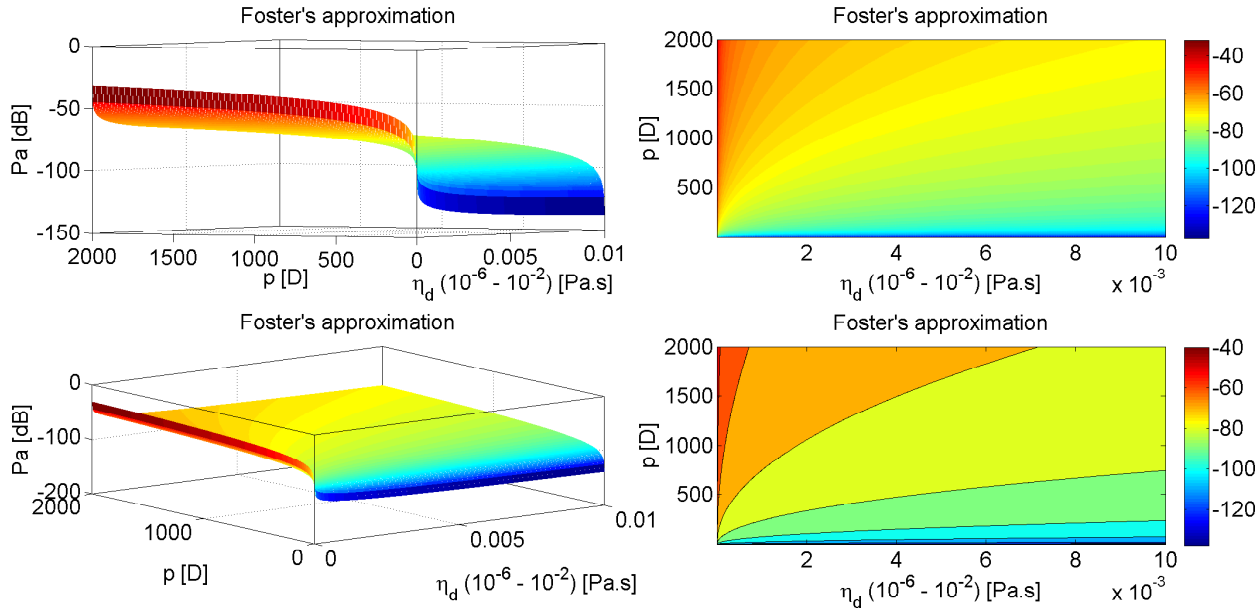

Fig. 34: Foster's absorption of 2 μm MTs in solution for various environment viscosity ($\eta_d = 10^{-6}$ - 10^{-2} Pa.s) and dipole moment (p = 0 - 2000 D) of tubulin heterodimer.

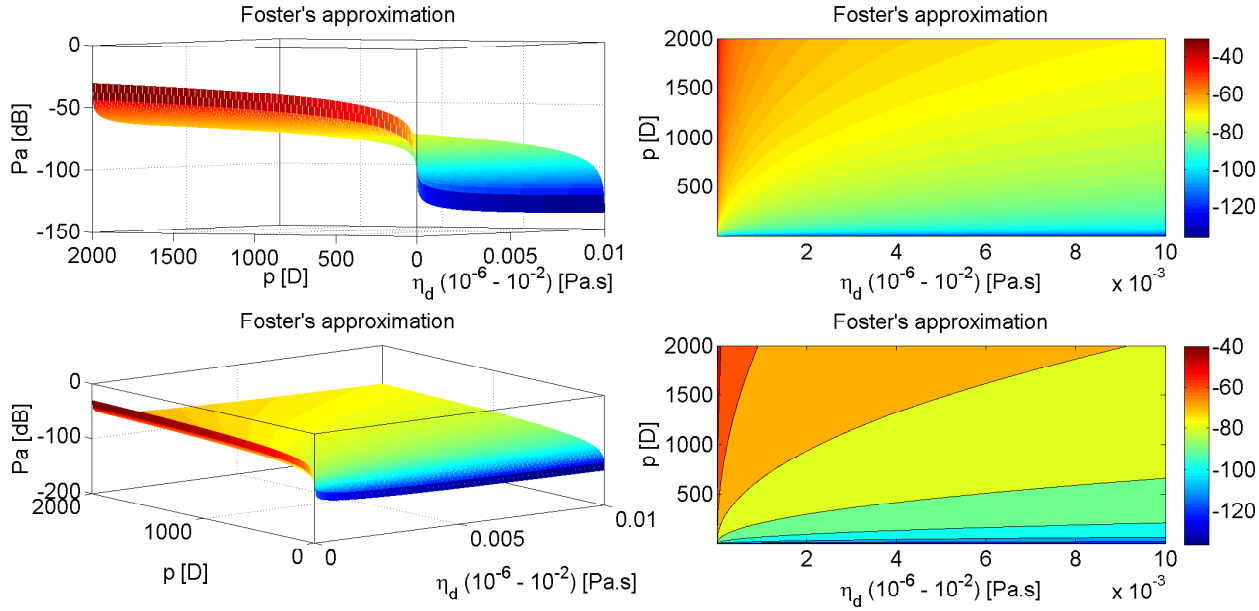

Fig. 35: Foster's absorption of 10 μm MTs in solution for various environment viscosity ($\eta_d = 10^{-6}$ - 10^{-2} Pa.s) and dipole moment (p = 0 - 2000 D) of tubulin heterodimer.

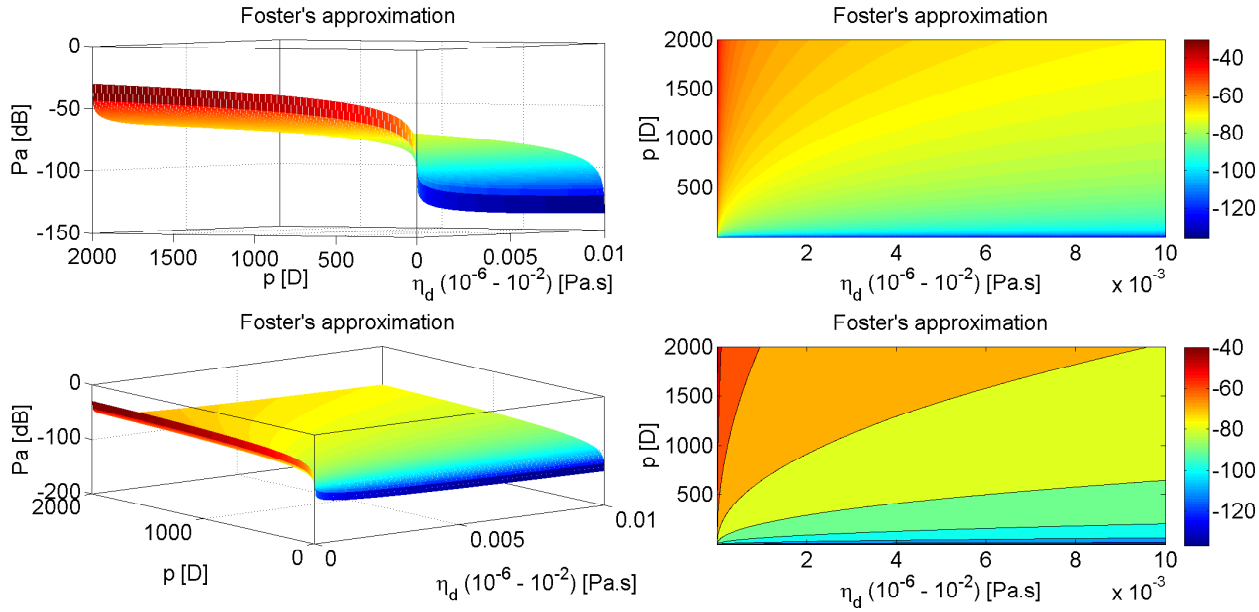

Fig. 36: Foster's absorption of 20 μm MTs in solution for various environment viscosity ($\eta_d = 10^{-6}$ - 10^{-2} Pa.s) and dipole moment (p = 0 - 2000 D) of tubulin heterodimer.

6.5 Absorption for MT population with various lengths

This subchapter gives the values of the absorbed power (P_a) for population of MTs with different lengths in a volume of 50 μl with 1 mg/ml concentration. The Gaussian distribution for length distribution was used, with mean value for MTs length 10 μm and the variance $\sigma = 10.10^{-6}$. Variance was chassed with respect to real MT lengths, maximum length was 50 μm, lengths lower than 0.5 μm were also cut off. The resulting values of absorbed power was determined from distribution fit by using the function *GEV* (Generalized Extreme Value). Results of calculations are shown in Figure 37.

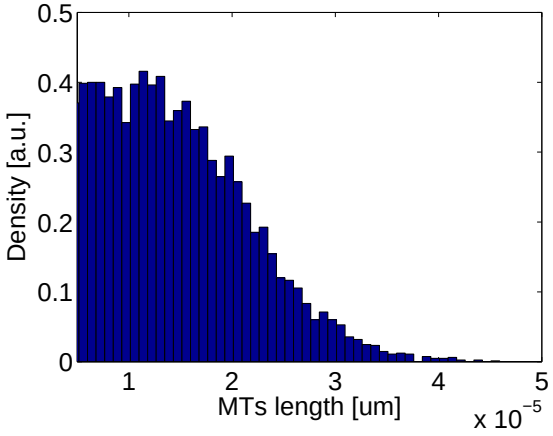

(a) Gaussian distribution of various MTs lengths.

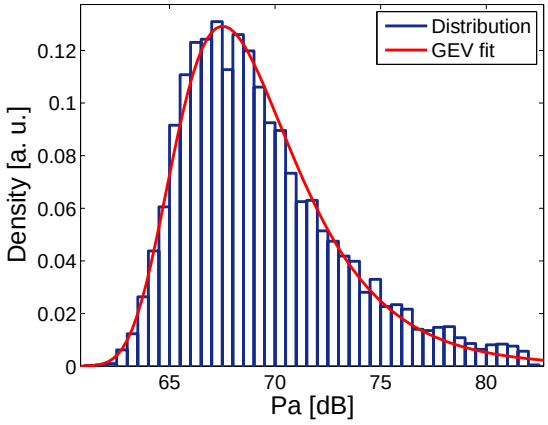

(b) Absorption of MTs in solution for various length distribution.

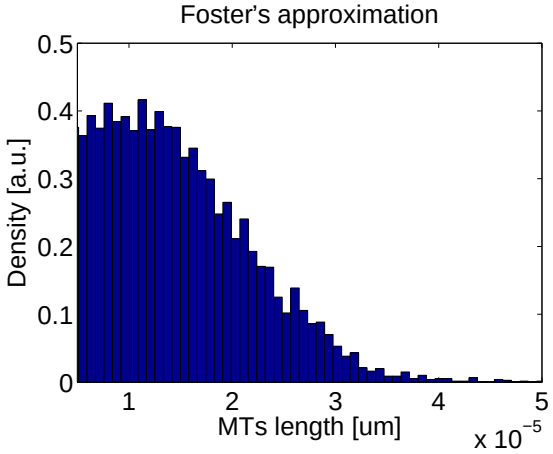

(c) Gaussian distribution of various MTs lengths.

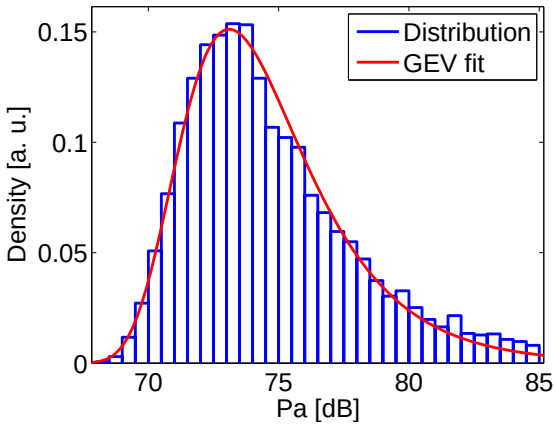

(d) Absorption of MTs in solution for various length distribution.

Fig. 37: Absorption of MTs in solution for various length distribution given by Gaussian distribution for Adair's and Foster's relaxation time calculations. ($p = 337$ D).

7 Protein permittivity in solution

This experimental section contains results of protein permittivity measurement in water solution. First Subchapter 7.1 describes biological samples which we used in our experiments. We specifically used the two types of Bovine Serum Albumin (BSA) in our experiments (described in Subchapter 7.1.1) with different purity and amount of impurities. Measurement setup and methodology are described in Subchapter 7.2 together with experimental results in Subchapter 7.3.

7.1 Biological samples

Bovine serum albumin was used as the biological sample. The purpose was to learn and establish reliable way of permittivity measurement in solution due to complexity of the experiment. It also gave us useful information about effects of protein to solution permittivity. After knowing the exact procedure and reliability of the experimental measurement the usage of tubulin will be considered. Bovine serum albumin is a serum albumin protein (Figure 38) derived from cows. It is often used as a protein concentration standard in lab experiments. Albumins are readily soluble in water and can only be precipitated by high concentrations of neutral salts such as ammonium sulfate. The solution stability of BSA is very good (especially if the solutions are stored as frozen aliquot). In fact, albumins are frequently used as stabilizers for other solubilized proteins (e.g., labile enzymes).

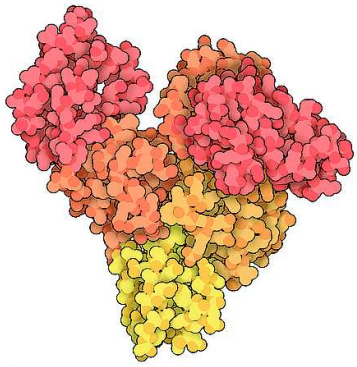

Fig. 38: Bovine Serum Albumin (PDB ID 3v03) crystal structure showing the 6 color-coded helical subdomains assembled to form the heart-shaped quaternary structure of the BSA protein molecule.

7.1.1 Bovine Serum Albumin

We used two different BSA proteins. The difference was in purity and in amount of impurities. First we used the lyophilized powder of BSA $\geq$96% (referred to as BSA1) and then lyophilized powder of BSA $\geq$98% (referred to as BSA2) from *Sigma-Aldrich*. Both of them was in form of lyophilized powder as was mentioned above plus BSA2 was essentially fatty acid free, essentially globulin free. The precise specifications of both proteins are described in Table 8.

BSA ≥96% (BSA1)				
Form	Loss on Drying	Nitrogen	Agarose Electrophoresis	pH
lyophilized powder	≤6%	14.5 - 16.5%	≥96%	6.7 - 7.3
BSA ≥98% (BSA2)				
lyophilized powder	≤5%	15.5 - 16.5%	≥98%	6.7 - 7.3

Tab. 8: Sigma - Aldrich specification of used BSA proteins.

7.2 Methodology and measurement procedure

Due to complexity of experimental measurement with different concentration of BSA protein in solution is this subsection divided into two independent parts. First subsection describes the exact procedure of sample preparation and final concentration with weights of BSA protein in individual solution 7.2.1. Second we introducing the description of measurement methodology and used aparature 7.2.2.

7.2.1 Sample preparation

Sample preparation was as follows. In order to be able to detect the permittivity change the high level of protein concentration is required. That is why we used high values of concentrations. We achieved these relatively high concentrations, by using relative small volumes of protein solutions (4 ml). We used deionized clean water as a medium. The exact concentrations and final volumes are summarized in Table 9.

BSA ≥96% (BSA1)				
Labeling	Concentration [%]	Protein quantity [mg/ml]	Final volume [ml]	Final quantity [mg/4ml]
BSA (96%) 5%	5	50	4	200
BSA (96%) 15%	15	150	4	600
BSA ≥98% (BSA2)				
BSA (98%) 5%	5	50	4	200
BSA (98%) 10%	10	100	4	400
BSA (98%) 15%	15	150	4	600
BSA (98%) 20%	20	200	4	800
BSA (98%) 25%	25	250	4	1000

Tab. 9: Table of used samples with calculated volumes and concentrations of protein.

We decided to measure samples of salt solutions due to impurity content in our protein powder. We thought that this salt impurities could have influenced permittivity. That is why we prepared samples of $NaCl$ and divalent $CaCl_2$ with same conductivities as BSA2 protein solutions. We measured conductivity of every protein solution and mix a NaCl and $CaCl_2$ solutions with same electric conductivities. Samples of salts are summarized in the Table 10. Conductivity was measured by $OrionSTAR$ A222 with $Orion$ 013010MD probe.

Electric conductivity [μS/cm] (23 °C)			
Labeling	BSA ≥98% (BSA2)	NaCl	$CaCl_2$
5% BSA2	125.5	126.3	126.2
10% BSA2	200.3	201.9	200.5
15% BSA2	317.0	318.1	301.5
20% BSA2	258.9	250.0	244.7
25% BSA2	212.1	201.9	200.5

Tab. 10: Electric conductivity of protein solutions, NaCl and $CaCl_2$ used in experiments measured by $OrionSTAR$ A222 with $Orion$ 013010MD probe at stable 23 °C.

From Table 10 we can se that the 10% and 25% BSA2 solution has nearly the same electrical conductivity. Therefore we prepared only four samples of NaCl and $CaCl_2$.

7.2.2 Experimental methodology and measurement procedure

We used the Agilent 85070E Dielectric Probe Kit which allowed us to measure complex permittivity over a broad frequency range starting from 200 MHz to 50 GHz. The Agilent 85070E Dielectric Probe Kit determines the dielectric properties, or complex permittivity, of many materials. Dielectric material properties are determined by its molecular structure. If the molecular structure changes, so will the dielectric properties. Measuring them can indirectly measure other properties that are also correlated to the molecular structure, and can be a valuable alternative when the property of interest is difficult to measure directly. The complete system was based on a network analyzer, which measures the material's response to RF or microwave energy. The probe transmits a signal into the tested material. We used Slim Form Probe, that allowed us to fit it easily in beaker and also allowed us to use smaller sample volume.

Sample volume was put into a glass beaker. Then we just simply inserted the probe into it with defined depth, to ensure that there will be at least 5 mm under and around the probe. We adjusted the depth of the dive by using the table with Y shift. We also compared the permittivity results of 15 ml water put into a bigger (infinite for probe) beaker to insure that the measured values are same as in the smaller beaker so we would minimize the measurement error (see Figure 40). The set-up, sample and probe dimensions are represented in Figure 39.

Before measuring, calibration at the tip of the probe was performed. A three-term calibration corrects for the directivity, tracking, and source match errors that can be present in a reflection measurement. In order to solve for these three error terms, we measured three well-known standards. The difference between the predicted and actual values was used to remove the systematic (repeatable) errors from the measurement. The three known standards were air, a short circuit, and distillate and de-ionized water. But even after calibrating the probe, there were additional sources of error that affected the accuracy of a measurement.

1. Cable stability during the calibration and measurement process.
2. Air Gaps, Air bubbles created at the end of the probe.
3. Sample thickness. The sample must also be thick enough to appear "infinite" to the probe.

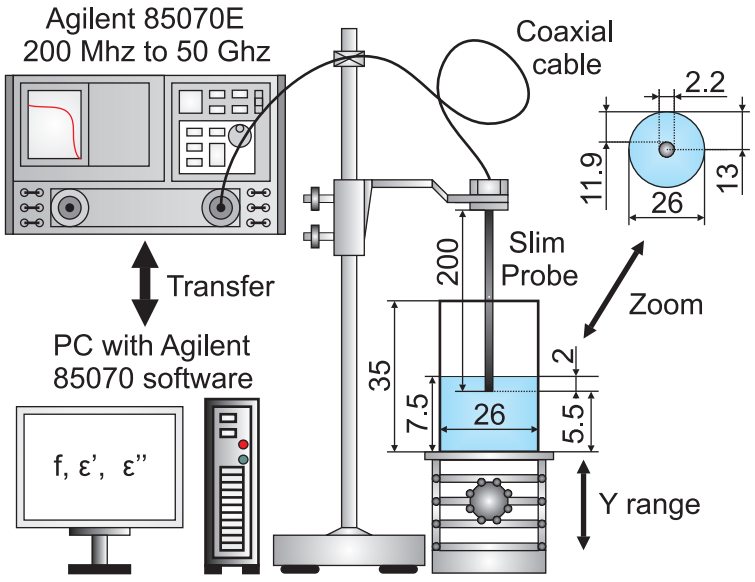

Fig. 39: Schematic representation of the measurement set-up, sample and coaxial probe dimensions (proportions are not to scale).

Coaxial cable was stabilized at all times of calibration and measurement due to noise and refraction errors at microwave frequencies which can influence the finite values of complex permittivity, mainly the imaginary part. After every measurement we executed Electronic Calibration Refresh which recalibrates the system automatically, just before each measurement was made. This virtually eliminated cable instability and system drift errors. Air bubbles which were created at the end of the probe were also one of the problems in measurement process. We tried to mix and wash the probe in a sample several times to insure that there are no bubbles at the end of it. But we cannot be absolutely sure, that there were no micro-bubbles at the end of the probe which could influenced the measurement. The sample size requirements for Slim Form Probe are 5 mm around tip of probe. We were trying to precisely insert the probe into the sample with defined height to meets these requirements.

Effect of small sample and probe position on complex permittivity is shown on Figure 40. From Figure 40 we can observe that there is small difference in real permittivity between the

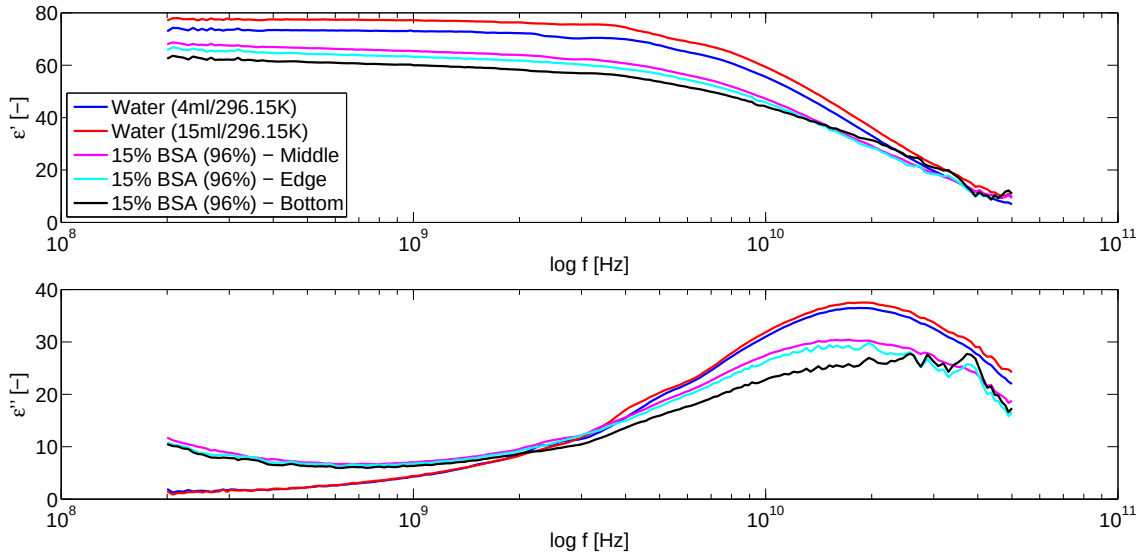

Fig. 40: Left: Effect of smaller volume of water on real and imag. part of complex permittivity. Right: Effect of probe position in beaker on real and imag. part of complex permittivity.

water with volume of 15 ml in bigger beaker than ours 4 ml sample. That is probably caused by the smaller volume of the sample and the size of the beaker. In imaginary part, there is no significant difference. We took this difference into account and we decided to repeat every measurement at least 3 times and determine the final value as the over all average. Then we tested influence of the probe position on the final permittivity. We can see that probe is not very sensitive to the position on the edge of the beaker, but is extremely sensitive to depth below. During the experiment we put probe at the bottom of the beaker and, there was a significant difference between permittivities (real and imaginary part too). That is why we tried to establish the exact depth of immersion so that there is at least 5 mm below the end of the probe a as it is requested in the manual from Agilent.

7.3 Experimental results

This Subsection contains experimental result of permittivity measurements. First we introduced the permittivity of BSA proteins in solutions (7.3.1), then we focused on permittivity of salts (NaCl, $CaCl_2$) (7.3.2) and at the end we made a comparison between the proteins and salts (7.3.3).

7.3.1 Permittivity of BSA protein in solutions

First we would like to introduce the results of BSA $\geq$96% (BSA1) protein in Figure 41, then BSA $\geq$98% (BSA2) protein in Figure 42. Third Figure 43 comparing permittivity of both proteins with same 5, 15% concentration. At the end we would also like to introduce permittivity dependence of BSA2 protein in solution on protein concentration (5, 10, 15, 20, 25 %) for four different frequencies (0.2, 1, 10, 40 GHz) in Fiugre 44.

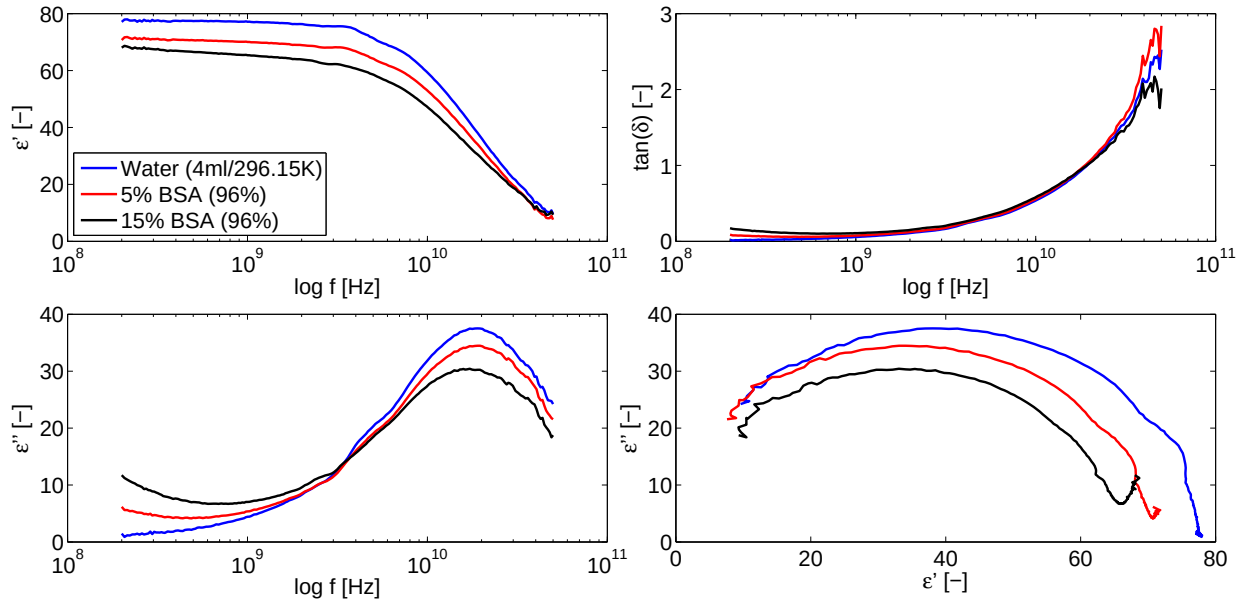

Fig. 41: Complex permittivities of BSA1 protein solutions with different concentrations (5, 15 %) in comparison with water solution at 23 °C from 200 MHz to 50 GHz.(Left: Real ($\varepsilon^{'}$) and Imaginary ($\varepsilon^{''}$) part of complex permittivity, Right: Dissipation factor (tan(δ)), Cole-Cole diagram).

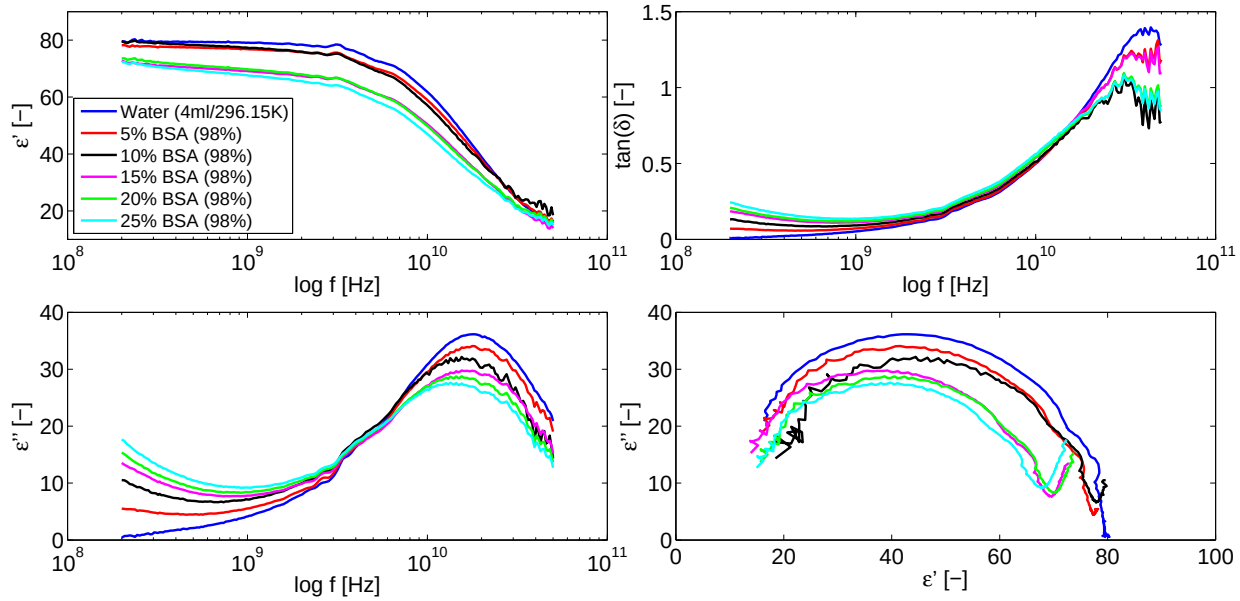

Fig. 42: Complex permittivities of BSA2 protein solutions with different concentrations (5, 10, 15, 20, 25 %) in comparison with water solution at 23 °C from 200 MHz to 50 GHz.(Left: Real ($\varepsilon^{'}$) and Imaginary ($\varepsilon^{''}$) part of complex permittivity, Right: Dissipation factor (tan(δ)), Cole-Cole diagram).

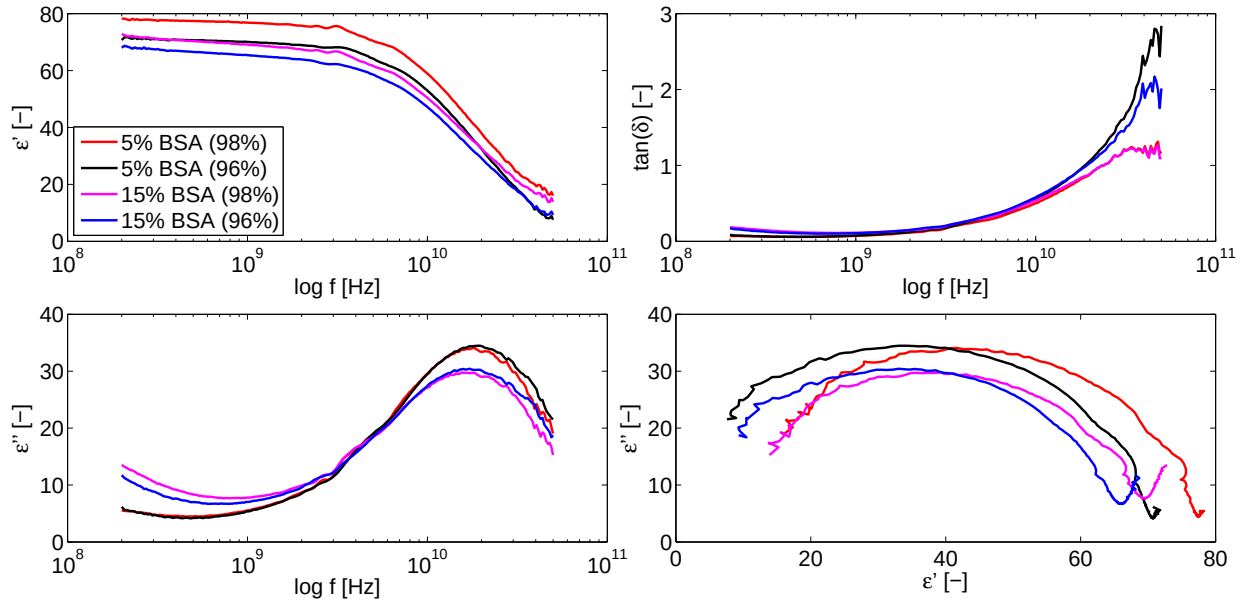

Fig. 43: Complex permittivity of BSA1 protein in comparison with BSA2 protein with same concentrations (5, 15%) in 4 ml water solutions at 23 °C from 200 MHz to 50 GHz.(Left: Real ($\varepsilon^{'}$) and Imaginary ($\varepsilon^{''}$) part of complex permittivity, Right: Dissipation factor (tan(δ)), Cole-Cole diagram).

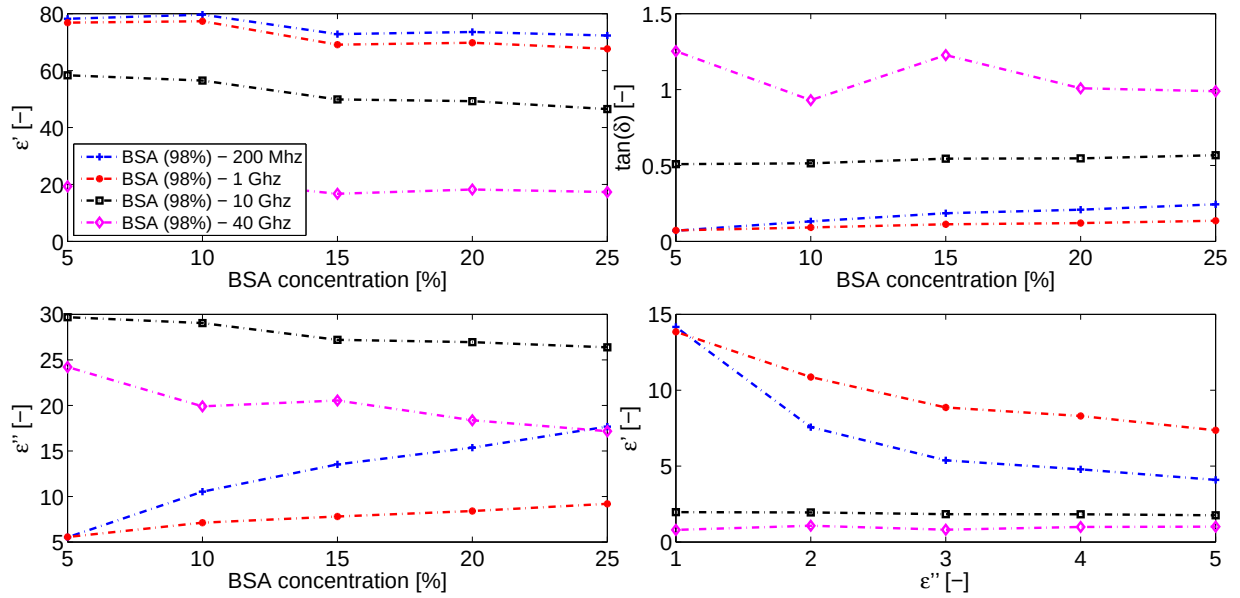

Fig. 44: Complex permittivity dependence of BSA2 solutions on protein concentrations (5, 10, 15, 20, 25 %) at 23 °C for four different frequencies (0.2, 1, 10, 40 GHz).(Left: Real ($\varepsilon^{'}$) and Imaginary ($\varepsilon^{''}$) part of complex permittivity, Right: Dissipation factor (tan(δ)), Cole-Cole diagram).

7.3.2 Permittivity of NaCl and $CaCl_2$

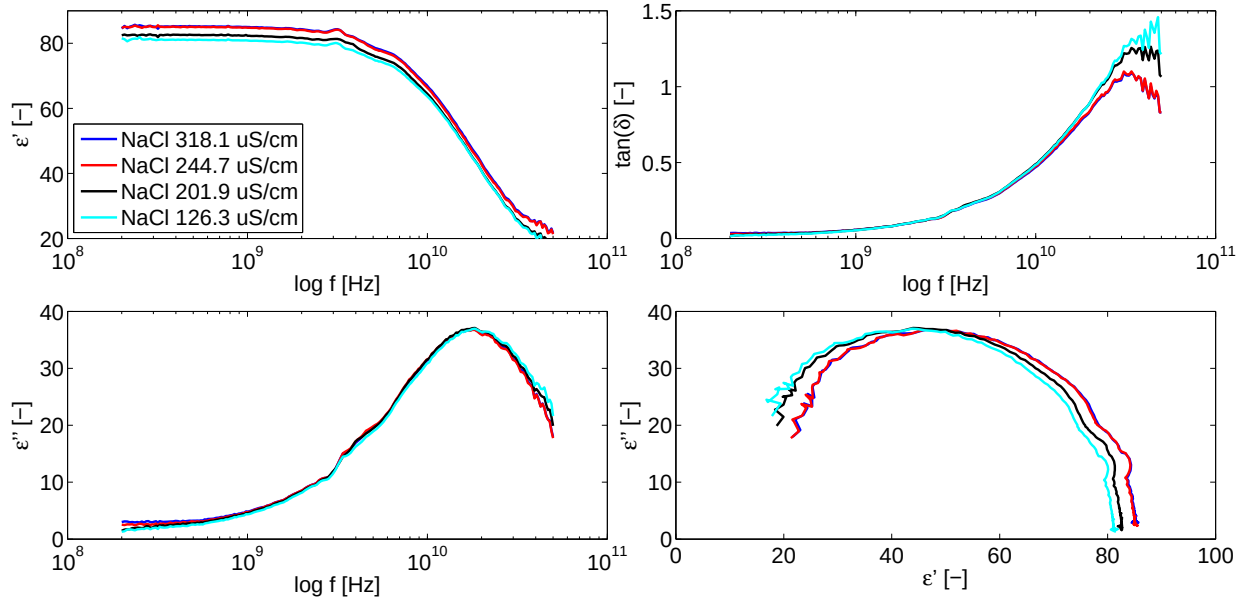

Fig. 45: Complex permittivities of NaCl solutions for 4 different conductivities at 23 °C from 200 MHz to 50 GHz.(Left: Real ($\varepsilon^{'}$) and Imaginary ($\varepsilon^{''}$) part of complex permittivity, Right: Dissipation factor (tan(δ)), Cole-Cole diagram).

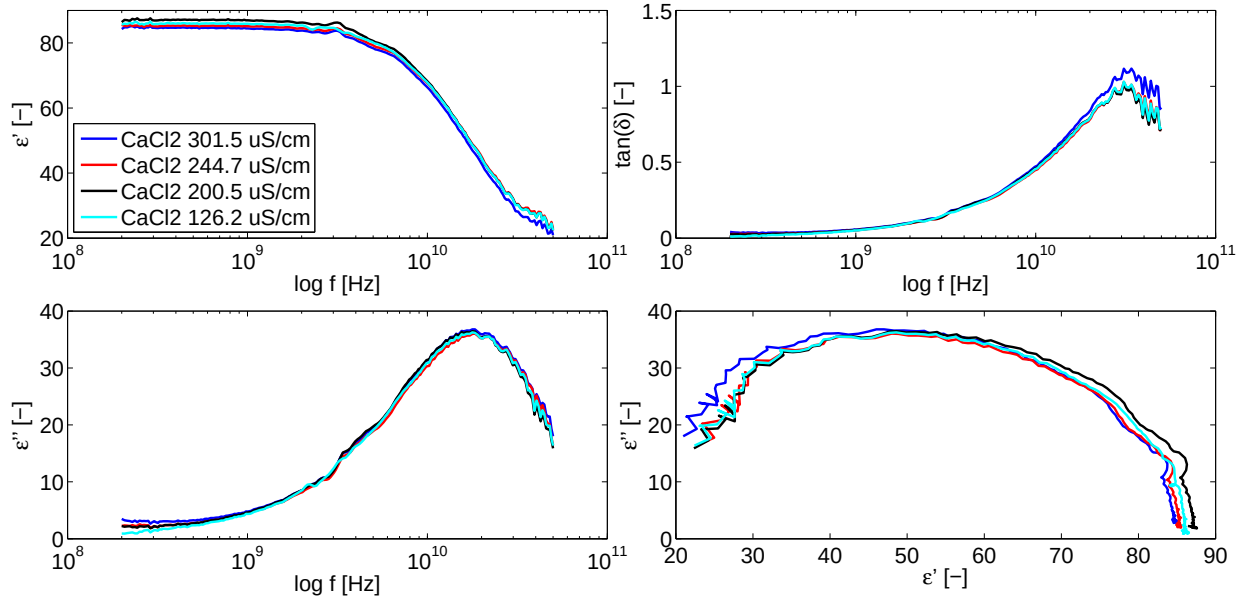

Fig. 46: Complex permittivities of $CaCl_2$ solutions for 4 different conductivities at 23 °C from 200 MHz to 50 GHz.(Left: Real ($\varepsilon^{'}$) and Imaginary ($\varepsilon^{''}$) part of complex permittivity, Right: Dissipation factor (tan(δ)), Cole-Cole diagram).

7.3.3 Permittivity comparison

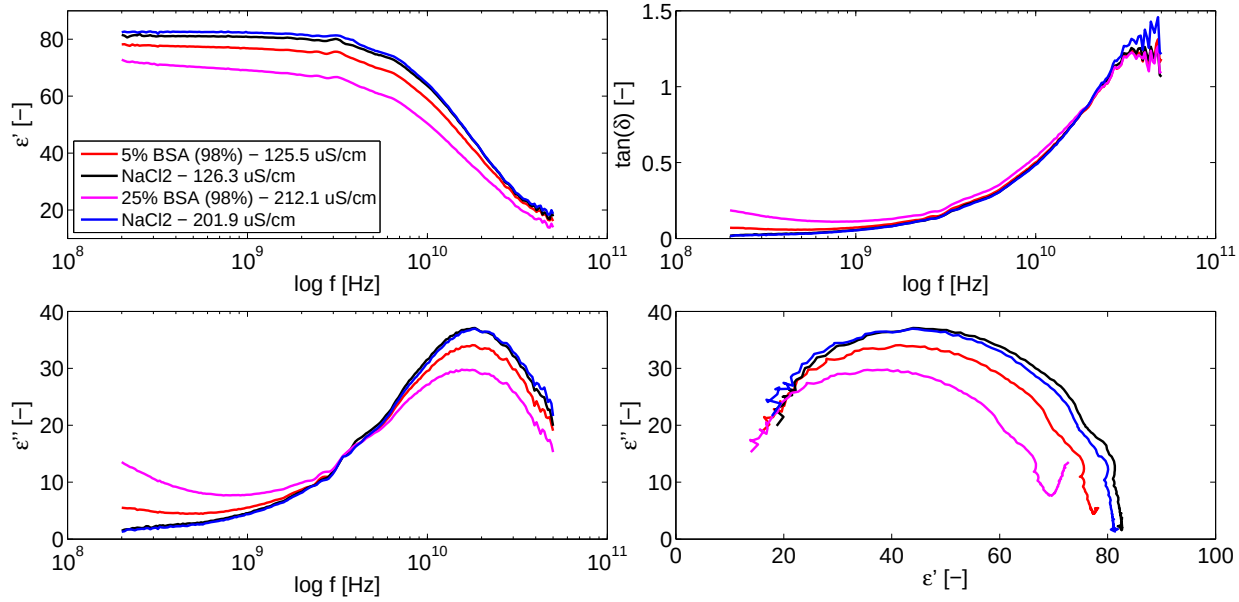

Fig. 47: Comparison of complex permittivities between BSA2 and NaCl solutions with same electrical conductivities at 23 °C from 200 MHz to 50 GHz.(Left: Real ($\varepsilon^{'}$) and Imaginary ($\varepsilon^{''}$) part of complex permittivity, Right: Dissipation factor (tan(δ)), Cole-Cole diagram).

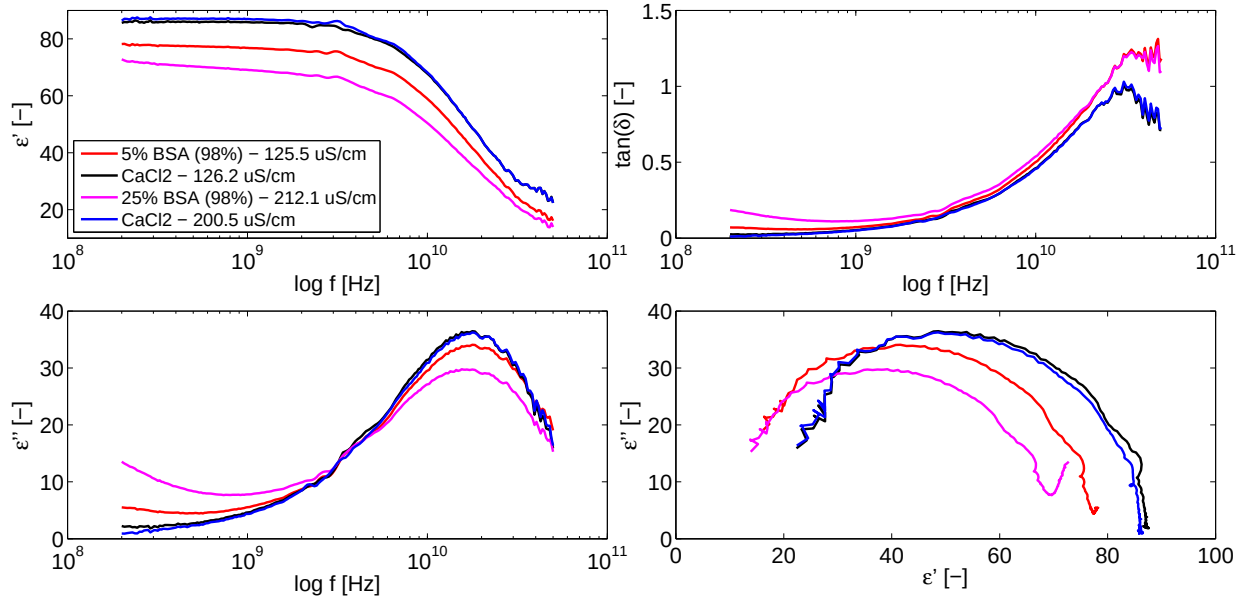

Fig. 48: Comparison of complex permittivities between BSA2 and $CaCl_2$ solutions with same electrical conductivities at 23 °C from 200 MHz to 50 GHz.(Left: Real ($\varepsilon^{'}$) and Imaginary ($\varepsilon^{''}$) part of complex permittivity, Right: Dissipation factor (tan(δ)), Cole-Cole diagram).

7.3.4 Permittivity model

This subsection contains the results of permittivity models described in Susection 3.7. First we made the model of water (Figure 49) permittivity based on Stogryn Equation (25). Then we applied this equation to protein model in Figure 50. Then we used Equation (26) with results in Figure 51. We can see that model well approximates the real part of complex permittivity. This model is valid also for an imaginary part considering it is measured in low protein concentration. The Debye relaxation model inaccuracy is determined by several factor. One of the main factors in creation of an accurate model is knowledge of permittivity in broad spectrum of frequencies including the MHz region. The second key factor is the protein concentration in the solution. Due to complexity of protein hydration and interaction with water ([20])it is hard to predict the protein behavior in high concentrations. Unfortunately, high-quality simulations of dielectric properties of solvated proteins are still limited to comparatively small solutes [25], [31], [6], [20]. Even if we have a low protein concentration, the knowledge of low frequencies permittivity play the key role in equations which includes all three protein processes (β, γ, δ).

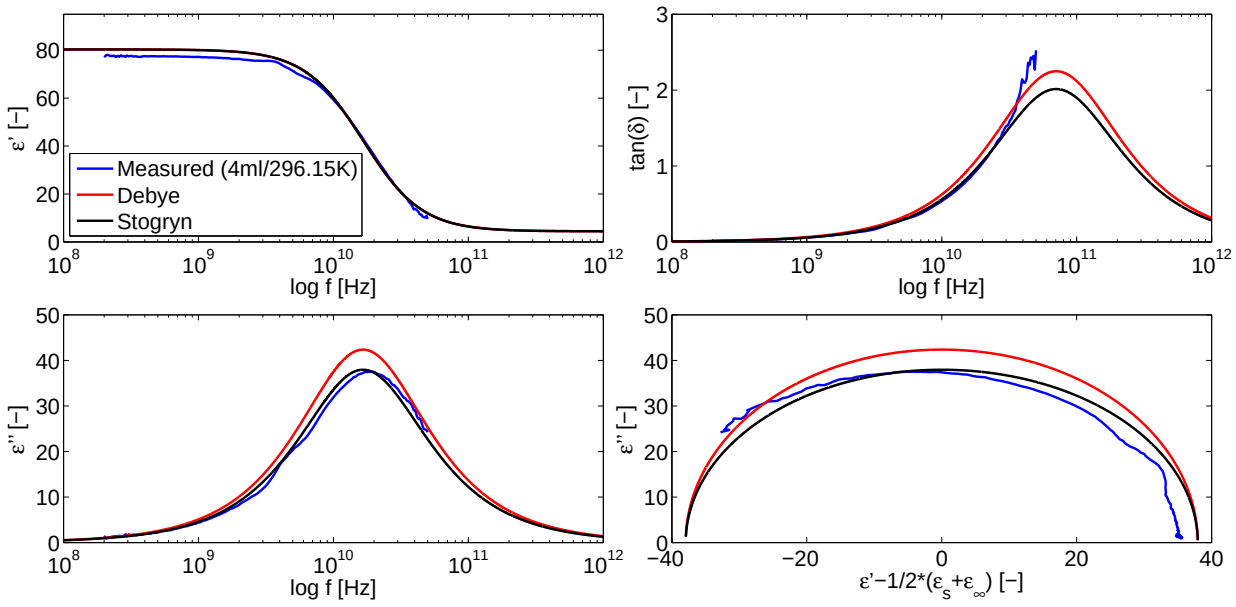

Fig. 49: Model of water permittivity based on Debye end Strogyn equations.(Left: Real ($\varepsilon^{'}$) and Imaginary ($\varepsilon^{''}$) part of complex permittivity, Right: Dissipation factor (tan(δ)), Cole-Cole diagram).

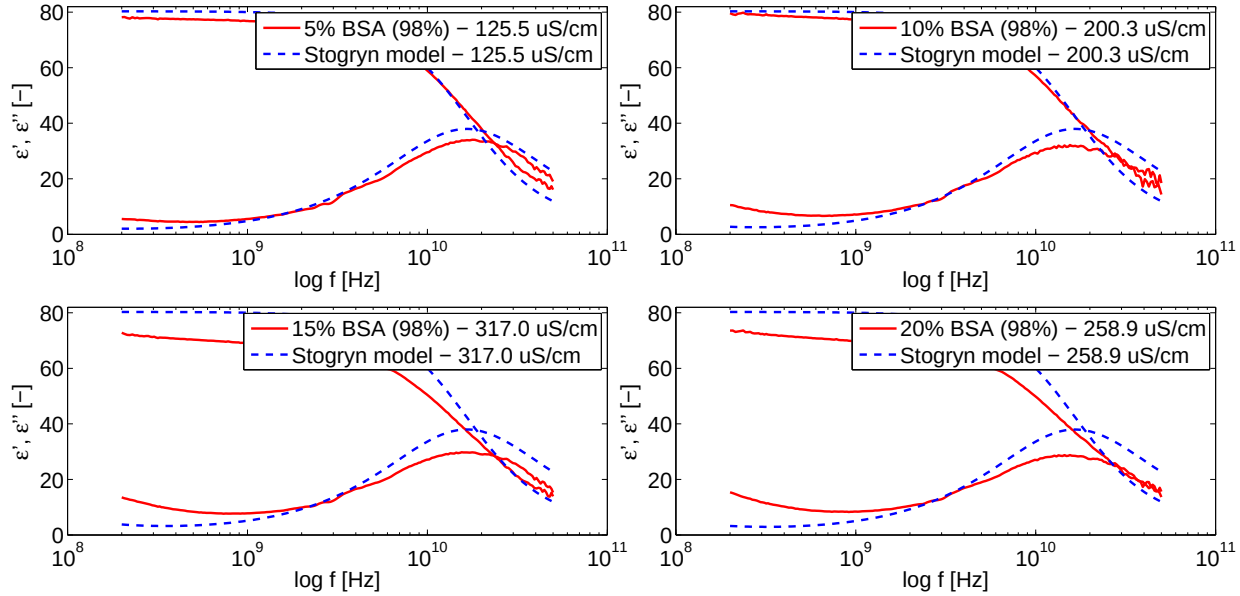

Fig. 50: Permittivity model of BSA protein in solutions by Stogryn equation with same electrical conductivities.

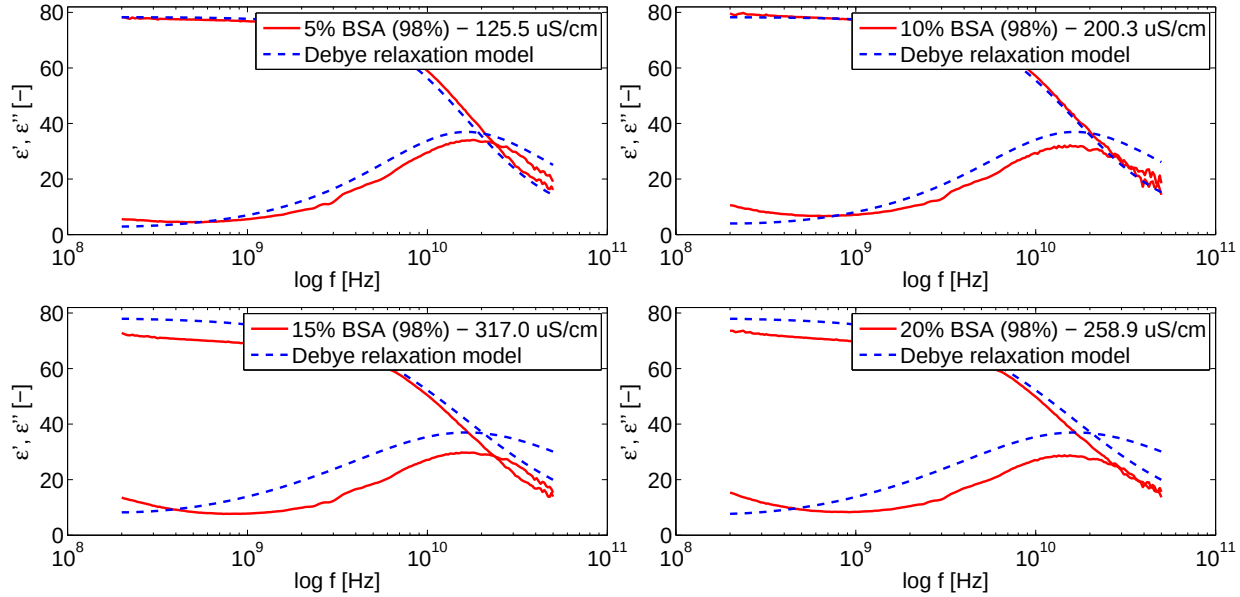

Fig. 51: Permittivity model of BSA protein in solutions by Debye relaxation model with same electrical conductivities.

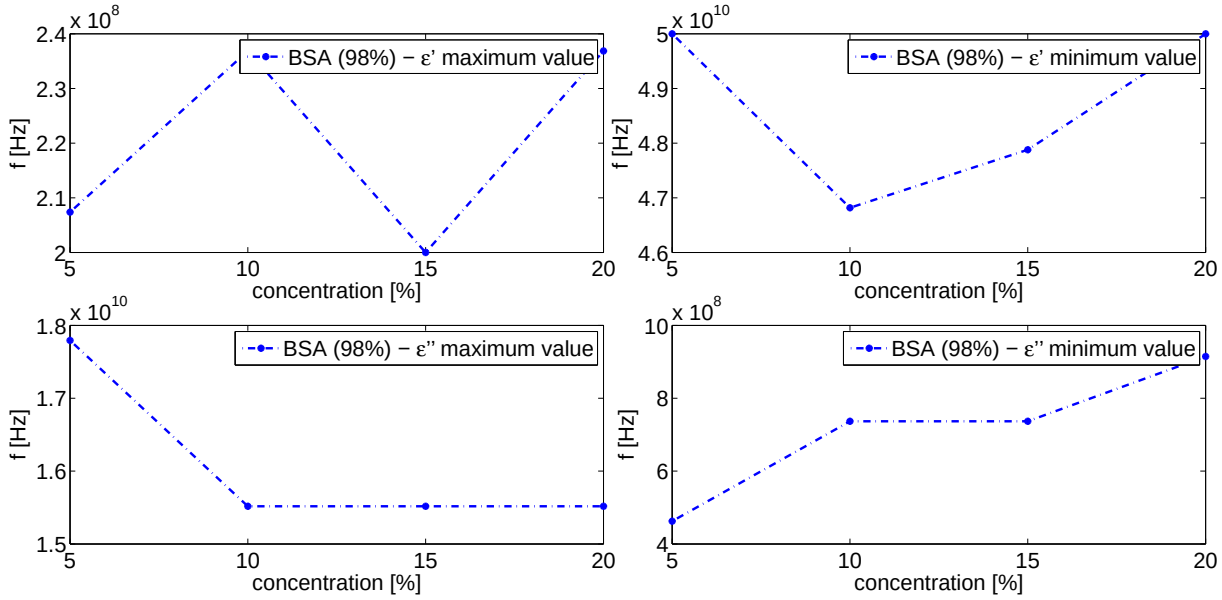

Fig. 52: Frequency comparisons of maximum and minimum values of Real and Img. part of complex permittivity for different BSA (98 %) concentrations.

7.4 Discussion of permittivity measurement

Complex permittivity of water seems to be influenced by the protein. From Figures 41 - 42 we can see that there is the moderate decrease of real part of complex permittivity with increasing concentration of protein. There is also decreasing trend in imaginary part of permittivity in higher frequencies, but also we can observe increased permittivity at lower frequencies. First we were assumed that this tendency was caused by presence of salt impurities in the BSA protein powder. That is why we made the measurement with NaCl and $CaCl_2$ salts (Figures 45 - 46). The results of comparison (Figures 47 - 48) indicate that this increase in imaginary part is not due to the presence of the salt in protein powder (mainly). Based on the theoretical knowledge about protein behavior in solutes we are currently assuming that this trend is caused by some minor contribution near 100 Hz of δ-process which had probably arisen either from the motion of the protein-bound waters, from protein water interactions, and/or from motions of polar side groups of the protein. We cannot confirm this fact due to the small frequency range of our measurement (0.2 - 50 GHz). We are also assuming, that there may be som other processes which could contribute to it. The decreasing trends can be also seen in Figure 44. What we are able to see from experimental results (decreasing trend of complex permittivity in real and imaginary part) in our frequency range is probably caused by presence of protein which is responsible for water retention which leads to smaller representation of water in sample. The main contribution to permittivity by proteins is in MHz region. For future work it would be very interesting for us to investigate the lower part of the spectrum in MHz region due to some protein processes which were described in Subsection 3.7.

8 Discussion

We reviewed theoretical study of microwave absorption in biological protein structure together with theoretical and experimental investigation of the protein influence on a complex permittivity in an aqueous solution. Microwave absorption by microtubules has been calculated. Calculations have shown that microtubule absorption is mainly dependent on its length, magnitude of dipole moment of tubulin heterodimer and on viscosity of the environment. In addition the effective dipole moment of tubulin heterodimer is dependent on the angle of rotation between the vector of the electric field and dipole moment. We used several techniques to the MT relaxation time calculation. Even if the power absorbed by single microtubule is relatively low we believe that absorption could play an important role in the protein structures and could have an impact on intracellular processes in the cell. Absorption results gave us useful information and better understanding of MT interaction with electromagnetic field and their possible role in generation of electromagnetic field. But all these theories and models will be beneficial only if we would be able to experimentally verified they truthfulness and support the development of its applications. Then we analyzed the influence of proteins on the permittivity of water. We found that permittivity of the environment is affected by presence of proteins, and it is related to the protein concentration. Presence of proteins in aqueous environment leads to a decreased value of the real part of complex permittivity in whole range of measured frequencies and to an increase of the imaginary part (at lower frequencies) due to a complex dispersion process in proteins. One of the reason was to establish reliable way of permittivity measurement and experimental results also gave us good starting point for understanding of protein - water interactions.
It would be interesting to create more precise absorption model of microtubules for different lengths and spatial distribution in water and simulate conditions in the cell. For future work we would like to investigate tubulin behavior in aqueous solution and its dielectric properties. After that the biggest challenge is to repeat dielectric measurement for polymerized microtubules. Dielectric properties of microtubules in solution should give us the answer about possible electromagnetic generation.

Appendix

Electrodynamic field in the cells

Ionic oscillation

An electrochemical model of ionic oscillations was proposed in the work by Pöhl where he suggested that cellular electrodynamic fields can be generated by the coupling of oscillating chemical reactions to the physically mobile ions within the regions of cell to produce charge waves [36]. In this model, oscillations of ions can be induced by chemical reactions, and the direction of oscillations will be steered by laminar and filamentous cellular structures. Pöhl's model of generation of cellular electrodynamic oscillations has not been developed further. Here it is interesting to note that many types of chemical reactions generate sound emission with spectra up to 1 MHz [13], thus oscillatory chemical processes up to this frequency can not be excluded. However, possibility of high frequency chemical oscillations in biologically relevant models is not known to current author.

Electronic oscillation

Possibility of oscillations of electrons in biomolecules is determined by electrical conductivity. Biomolecule which is known to conduct electrons is DNA [16]. In the case of DNA, it is so called phonon assisted conductivity, i.e. conductivity attributed to polarons [7], quasiparticles which involve charge (here electron) and associated deformation of the lattice (cloud of phonos). DNA polaron-based conductivity is now widely and intensively studied scientific field. Due to its conductive properties, DNA has been labeled by one collective of authors even as an antenna for electromagnetic field [13]. Proteins were generally accepted to be nonconducting for long time while some theoretical predictions propose conduction or semiconduction to occur in them.

Mechanical vibrations of electrically polar structures

The third of approaches for electrodynamic field of the cell is based on the vibrations of electrically polar biomolecular cellular structures. The vibrating modes of biomolecules have been studied by several types of spectroscopy [5].
The frequency of vibration depends on the size and rigidity of the structure [26], as well as on the type of vibration mode. It is also known that the cell contains either the internal structure of the electrically polar (most proteins is electrically polar), or structures such as membranes, which are electrically polarized to different electric potential on their sides. The basic idea is that metabolic energy produces vibrations electrically polar molecules that generate cell electrodynamic field. The following text describes the theory of Herbert Fröhlich, who postulated the possibility of generation of electromagnetic field in biological systems under certain specific conditions on the basis of mechanical vibrations electrically polar structures.

References

[1] Robert K. Adair. Vibrational resonances in biological systems at microwave frequencies. *Biophysical Journal*, 82(3):1147–1152, 2002.

[2] B. Alberts, D. Bray, and A. Jonhson. *Základy buněčné biologie*. Espero Publishing, second edition, 2005.

[3] Mélis Arslan. *Micromechanical Modeling of Microtubules*. Doctoral thesis, Paris Institute of Technology, January 2010.

[4] Malvin Carl Teich Bahaa E. A. Saleh. Základy fotoniky i. Matfyzpress, 1996.

[5] Andreas Barth. Infrared spectroscopy of proteins. *Biochimica et Biophysica Acta (BBA) - Bioenergetics*, 1767(9):1073 – 1101, 2007.

[6] T. H. Basey-Fisher, S. M. Hanham, H. Andresen, S. A. Maier, M. M. Stevens, N. M. Alford, and N. Klein. Microwave debye relaxation analysis of dissolved proteins: Towards free-solution biosensing. *Applied Physics Letters*, 99(23), 2011.

[7] Goodman R. Blank M. Dna is a fractal antenna in electromagnetic fields. *International journal of radiation biology*, 87:409–415, 2011.

[8] J.M. Blatt and V.F. Weisskopf. *Theoretical Nuclear Physics*. Dover Books on Physics Series. Dover Publications, 1991.

[9] Konrad J. Bohm, Nikolaos E. Mavromatos, Alan Michette, Roland Stracke, and Eberhard Unger. Movement and alignment of microtubules in electric fields and electric-dipole-moment estimates. *Electromagnetic Biology and Medicine*, 24(3):319–330, 2005.

[10] Jonathan Andrew Marc Brown. *A Study of the Interactions between Electromagnetic Fields and Microtubules: Ferroelectric Efects, Signal Transduction and Electronic Conduction*. Doctoral thesis, University of Alberta, Edmonton Alberta, May 1999.

[11] M. Cifra, J. Pokorný, D. Havelka, and O. Kucera. Electric field generated by axial longitudinal vibration modes of microtubule. *Biosystems*, 100(2):122–131, 2010.

[12] Michal Cifra. *Study of electromagnetic oscillations of yeast cells in kHz and GHz region*. Doctoral thesis, Czech Technical University, Prague, July 2009.

[13] Michal Cifra, Jeremy Z. Fields, and Ashkan Farhadi. Electromagnetic cellular interactions. *Progress in Biophysics and Molecular Biology*, 105(3):223–246, 2010.

[14] J.T. Edsall and H.A. McKenzie. Water and proteins. the location and dynamics of water in protein systems and its relation to their stability and properties. *Advances in Biophysics*, 16(0):v – vi, 1983.

[15] Richard P. Feynman, Robert B. Leighton, and Matthew Sands. *Feynmanovy přednášky z fyziky s řešenými příklady 2/3*. Fragment, first edition, 2001.

[16] Hans-Werner Fink and Christian Schonenberger. Electrical conduction through dna molecules. *Nature*, 398(6726):407–410, 1999.

[17] Hannes Fischer, Igor Polikarpov, and Aldo F. Craievich. Average protein density is a molecular-weight-dependent function. *Protein Science*, 13(10):2825–2828, 2004.

[18] Kenneth R. Foster and James W. Baish. Viscous damping of vibrations in microtubules. *Journal of Biological Physics*, 26(4):255–260, 2000.

[19] Matthew P. Goertz, J. E. Houston, and X.-Y. Zhu. Hydrophilicity and the viscosity of interfacial water. *Langmuir*, 23(10):5491–5497, 2007.

[20] Bertil Halle. Protein hydration dynamics in solution: a critical survey. *Philosophical Transactions of the Royal Society of London. Series B: Biological Sciences*, 359(1448):1207–1224, 2004.

[21] D. Havelka, M. Cifra, O. Kucera, J. Pokorný, and J. Vrba. High-frequency electric field and radiation characteristics of cellular microtubule network. *Journal of Theoretical Biology*, 286:31–40, 2011.

[22] Daniel Havelka. Elektromagnetické pole mikrotubulárního systému buňky. Master thesis, Czech Technical University, Prague, March 2010.

[23] Miloš Mazánek Pavel Pechač Karel Novotný, Zbyněk Škvor. *Vlny a vedení*. 2008.

[24] Jung-Mu Kim, Dong Hoon Oh, Jae-Hyoung Park, Jei-Won Cho, Youngwoo Kwon, Changyul Cheon, and Yong-Kweon Kim. Permittivity measurements up to 30 ghz using micromachined probe. *Journal of Micromechanics and Microengineering*, 15(3):543–550.

[25] A. Knocks and H. Weingartner. The dielectric spectrum of ubiquitin in aqueous solution. *The Journal of Physical Chemistry B*, 105(17):3635–3638, 2001.

[26] Ondrej Kucera and Daniel Havelka. Mechano-electrical vibrations of microtubules - link to subcellular morphology. *Biosystems*, 109(3):346–355, 2012.

[27] Harvey Lodish, Arnold Berk, and Chris A. Kaiser. *Molecular Cell Biology*. Katherine Ahr Parker, seventh edition, 2012.

[28] E M Mandelkow, E Mandelkow, and Milligan. Microtubule dynamics and microtubule caps: a time-resolved cryo-electron microscopy study. *The Journal of Cell Biology*, 114(5):977–991, 1991.

[29] A. Mershin, A. A. Kolomenski, H. A. Schuessler, and D. V. Nanopoulos. Tubulin dipole moment, dielectric constant and quantum behavior: computer simulations, experimental results and suggestions. biosystems. 2004.

[30] Pavel Pechač Miloš Mazánek. *Šíření elektromagnetických vln a antény*. 2008.

[31] Nobuhiro Miura, Nobuyuki Asaka, Naoki Shinyashiki, and Satoru Mashimo. Microwave dielectric study on bound water of globule proteins in aqueous solution. *Biopolymers*, 34(3):357–364, 1994.

[32] Haruki Nakamura and Akiyoshi Wada. Nature of the charge distribution in proteins electric multipole structures. *Journal of the Physical Society of Japan*, 54(10):4047–4052, 1985.

[33] E. Nogales, S.G. Wolf, and K.H. Downing. Structure of the alpha beta tubulin dimer by electron crystallography. *Nature*, 391(6663):199–203, 1998.

[34] Eva Nogales, Sharon G. Wolf, and Kenneth H. Downing. Structure of the tubulin dimer by electron crystallography. *Nature*, 391(6663):199–203, 1998.

[35] Ivan Richter Pavel Fiala. Fyzikální optika. ČVUT, 2005.

[36] Herbert A. Pohl, Tim Braden, Scott Robinson, Jayne Piclardi, and Douglas G. Pohl. Life cycle alterations of the micro-dielectrophoretic effects of cells. *Journal of Biological Physics*, 9(3):133–154, 1981.

[37] J. Pokorný. Excitation of vibrations in microtubules in living cells. *Bioelectrochemistry*, 63(1-2):321–326, 2003.

[38] Jiří Pokorný. Viscous effects on polar vibrations in microtubules. *Electromagnetic Biology and Medicine*, 22(1):15–29, 2003.

[39] Jiří Pokorný, František Jelínek, and Viktor Trkal. Electric field around microtubules. *Bioelectrochemistry and Bioenergetics*, 45(2):239–245, 1998.

[40] Bedřich Sedlák and Ivan Štoll. *Elektřina a magnetismus*. Karolinum, third edition, 2012.

[41] A. Stogryn. Equations for calculating the dielectric constant of saline water (correspondence). *Microwave Theory and Techniques, IEEE Transactions on*, 19(8):733–736, Aug 1971.

[42] R Stracke, K.J Bohm, L Wollweber, J.A Tuszynski, and E Unger. Analysis of the migration behaviour of single microtubules in electric fields. *Biochemical and Biophysical Research Communications*, 293(1):602–609, 2002.

[43] Jedrzej Szymański, Adam Patkowski, Agnieszka Wilk, Piotr Garstecki, and Robert Holyst. Diffusion and viscosity in a crowded environment: from nano- to macroscale. *The Journal of Physical Chemistry B*, 110(51):25593–25597, 2006.

[44] Ivan Štoll. Elektřina a magnetizmus. ČVUT, 2003.

[45] J.A. Tuszynski, J.A. Brown, E. Crawford, E.J. Carpenter, M.L.A. Nip, J.M. Dixon, and M.V. Satariat. Molecular dynamics simulations of tubulin structure and calculations of electrostatic properties of microtubules. *Mathematical and Computer Modelling*, 41(10):1055 – 1070, 2005. Modelling Complex Systems in Molecular Biology and Tumor Dynamics and Control.

[46] Peter M. Vassilev, Reni T. Dronzine, Maria P. Vassileva, and Georgi A. Georgiev. Parallel arrays of microtubles formed in electric and magnetic fields. *Bioscience Reports*, 2(12):1025–1029, 1959.

[47] Radim Zajíček. *Application of Complex Permittivity Measurement in Medical Diagnostics and Imaging*. Doctoral thesis, Czech Technical University, August 2009.